scientific reports

Check for updates

OPEN

CSP ubiquitylation favours *Plasmodium berghei* survival during early liver stage infection

Sara J. S. Baptista[1,2], Aparajita Lahree[2,3], Sofia Marques[1,2], Inês Bento[1,2], João Mello-Vieira[2,4], António M. Mendes[2,5], Vanessa Zuzarte-Luís[2,5] & Maria M. Mota[1,2]✉

The circumsporozoite protein (CSP), an essential protein that covers the surface of the *Plasmodium* sporozoite, is a key player in multiple stages of the parasite development within the mosquito and during interactions between sporozoites and mammalian hepatocytes. Here, we identify a novel function of *Plasmodium berghei* CSP: preventing parasite elimination during the early stages of hepatic infection, through its ubiquitylation at two lysine (K) residues, K252 and K258, located in the C-terminal domain. A *Plasmodium berghei* transgenic line lacking these lysine residues exhibited a significant decrease in hepatic infectivity, with parasites being eliminated 4 h after infection. The reduced infectivity correlated with an increased association of host autophagy markers, LC3 and LAMP1, to the parasitophorous vacuole membrane of the liver stage parasite. Notably, inhibiting the host autophagy pathway fully rescued the mutant parasites from elimination. Collectively, we reveal a strategy employed by *Plasmodium* to evade early clearance during hepatic infection, which relies on the ubiquitylation of specific CSP lysine residues, that results in reduced parasite elimination via host autophagic and lysosomal activity.

Malaria is an ancient disease that continues to be a major public health concern, particularly in endemic areas of sub-Saharan Africa[1]. *Plasmodium* parasites are the causative agents of malaria, where they infect and multiply inside red blood cells (RBCs), giving rise to disease symptoms. In mammals, *Plasmodium* is delivered into the host by the bite of an infected female *Anopheles* mosquito. This infectious form, the sporozoite, migrates to the liver and develops in hepatocytes, the liver stage of infection, where its replication occurs to generate RBCs-infectious forms, the merozoites, that once in the blood originate the symptoms. The clinical disease, hence, depends on the capacity that sporozoites have to successfully invade and mature as a liver stage within a hepatocyte[2].

The surface of *Plasmodium* sporozoites is covered by a dense coat of the circumsporozoite protein (CSP), which is highly conserved across *Plasmodium* species infecting mammals, including humans[3,4]. CSP plays a dominant role in sporogony[5], sporozoite migration from mosquito to mammalian host[6], sporozoite arrest in the liver[7], and hepatocyte invasion [8–10].

CSP has a N-terminus conserved domain (region I), which upon cleavage allows hepatocyte invasion in vitro, suggesting that CSP processing on the sporozoite surface is required for active sporozoite invasion[4,11]. The species-specific CSP central repeat region consists of a tandem repeat of amino acids commonly found in reverse turns. This region corresponds to half of the CSP's amino acid sequences and the replacement of the endogenous CSP locus with a mutant version lacking the repeat region results in the degeneration of sporozoites during their development in the mosquito[12]. Lastly, the CSP C-terminal end is composed mainly of hydrophobic amino acids[4], (region II (RII)), known as TSR region, and a GPI anchor site, which is required for the surface localization of CSP in oocysts/sporozoites and for sporozoite development[13].

Proteins of diverse intracellular pathogens undergo post-translational modifications (PTMs) that are critical to modulate infection[14]. PTMs are enzymatically driven modifications, that either "add" or "cleave" amino acids or chemical groups from native proteins after their translation in the ribosome originating a wider proteome from the number of proteins encoding genes. PTMs can be site-specific modifications such as an addition of (i) chemical/ionic groups (such as phospo, acetyl, methyl, O-GlcNAc, etc.), (ii) more complex polypeptides (such as

[1]Gulbenkian Institute for Molecular Medicine, 1649-028 Lisbon, Portugal. [2]Instituto de Medicina Molecular JLA, Universidade de Lisboa, 1649-028 Lisbon, Portugal. [3]Max-Planck-Institute of Molecular Cell Biology and Genetics, Pfotenhauerstrasse 108, Dresden, Germany. [4]Faculty of Medicine, Institute of Biochemistry 2 and Buchmann Institute for Molecular Life Sciences, Goethe University Frankfurt, Frankfurt, Germany. [5]SGS Portugal S.A., Polo Tecnológico de Lisboa, R. Cesina Adães Bermudes Lote 11 N° 1, 1600-604 Lisbon, Portugal. ✉email: maria.mota@gimm.pt

ubiquitylation, ISGglylation, neddylation and sumoylation) and (iii) carbohydrate or lipid molecules (including, glycosylation, ADP-ribosylation, palmitoylation, myristoylation and prenylation)[15].

Most PTM studies in pathogens focus on phosphorylation and acetylation. Ubiquitylation, the second most common PTM after phosphorylation, remains poorly understood[16]. In *Plasmodium* the role of protein ubiquitylation has been mainly addressed on parasite development within RBCs[17–20]. The dynamics of CSP PTMs remain poorly understood, with a single study showing that CSP glycosylation is important for the colonization of the mosquito salivary glands by *P. falciparum* sporozoites[21]. This study utilized advanced proteomic approaches to identify O-fucose or O-glucosylfucose disaccharides on CSP Threonine337 as key to promote sporozoite survival, motility, and interactions with host tissues within the mosquito vector, highlighting the broader importance of CSP PTMs in the parasite's life cycle and its interactions with the host.

At the center of ubiquitylation is the conserved and abundant 76 amino acid polypeptide- ubiquitin. Ubiquitylation involves the reversible covalent attachment of single, or multiple ubiquitin molecules linked via lysine (K) residues, to a K residue in the target protein[14,15]. The fate of the target protein is dictated by the type of tagging, (mono- vs poly-ubiquitylation chains) and the lysine residues involved in the branching, being common the targeting of the proteins for degradation via proteasome. The ubiquitin-proteasome system (UPS) is the most common pathway for degradation of polyubiquitylated proteins, by recognizing and degrading substrates containing polyubiquitin chains with a minimum of four ubiquitin molecules linked via their K48 residues. Ubiquitylation for proteasome delivery not only controls protein turn-over by degradation but also several cell cycle checkpoints and signaling networks of the innate and adaptive immune responses against pathogens, including inflammatory signaling, apoptosis, and autophagy, which are known to eliminate *Plasmodium* parasites[22–24] and other intracellular pathogens[14,25].

Cumulative evidence proposes ubiquitylation as a prevalent and relevant PTM connecting the two major degradation and recycling systems in eukaryotes – the UPS and macroautophagy (henceforth, referred to as autophagy)[26]. Autophagy is an intracellular degradation system where autophagy-related gene products coordinate the formation of autophagosomes that sequester cytoplasmic cargo and deliver the cargo to lysosomes for the degradation of its contents through the activities of lysosomal hydrolases[14,27]. Typically, unwanted larger cytosolic structures are selectivity degraded by either ubiquitin-independent (direct binding of the autophagy receptors to intracellular cargo) or ubiquitin-dependent autophagy[14,27]. In selective autophagy, the ubiquitin like microtubule-associated protein 1 light chain 3 (LC3) is an essential autophagy marker, whereas the autophagic cargo receptors, in particular sequestosome 1 (also known as p62/SQSTM1, and hereafter referred to as p62) is the major driver of ubiquitin condensate formation that mediates the recruitment of ubiquitylated proteins into autophagosomes[28]. The degradation of cytoplasmic proteins and organelles through autophagy is critically dependent on lysosomal proteolysis. The endolysosomal system is an integral component of the cellular catabolic machinery, responsible for processing and recycling nutrients required for the synthesis of biomaterials. It also functions as a signaling hub, coordinating the cellular energy state with growth and differentiation processes[29]. A key characteristic of a mature lysosome is its limiting membrane, which contains specific glycosylated membrane-associated proteins, such as LAMP1 and LAMP2 (lysosomal-associated membrane protein 1/2). In vertebrates, these proteins are ubiquitously expressed and constitute approximately 50% of the lysosomal membrane proteins[29].

Here, we explored the physiological impact of *Plasmodium berghei* (*Pb*) CSP ubiquitylation in the host, for parasite liver stage clearance in coordination with host autophagy and lysosomal acidification activity during the early hours of the exoerythrocytic stage of infection.

Results

Pb CSP is ubiquitylated by host hepatocytes

We first aimed to evaluate the status of *Pb* CSP ubiquitylation during exoerythrocytic infection. For that, HepG2 cells were treated with a commercial proteasome inhibitor (MG132) that blocks proteasome activity[30], leading to the accumulation of ubiquitylated proteins during *Pb* sporozoites infection. For prior testing, we established that the selected concentration of MG132 used in these assays (10 µM), did not impair the sporozoite's ability to traverse, invade, and establish inside hepatocytes (Supplementary Fig. 1a-c, respectively). At 4 h post-infection (hpi), we immunoprecipitated ubiquitin in *Pb*-infected HepG2 cells with or without proteasome blockage and monitored CSP accumulation by Western Blot (WB). Immunoprecipitation was performed using an anti-ubiquitin antibody with affinity for mono and polyubiquitylated proteins, irrespective of the linkage type. CSP accumulation in *Pb*WT-infected HepG2 cells could only be observed upon proteasome inhibition (Fig. 1a).

To exclude the interference of other parasite proteins in the ubiquitylation of *Pb* CSP by the host ubiquitin–proteasome system (UPS), we established an artificial ubiquitylation system, as used by others in the study of mammalian UPS interactions with proteins of intracellular pathogens[31,32]. To this end, we used a transient transfection system in which a plasmid containing HA-tagged codon-optimized *Pb* ANKA WT CSP gene (pHA-*Pb*CSP^{WT}) was transfected into human embryonic kidney (HEK) 293 T cells, along with a histidine-tagged ubiquitin construct (pHis^{6}-ub)[33]. Ubiquitylated CSP was obtained from total cellular lysates using a nickel-nitrilotriacetic acid (Ni–NTA) pull-down in the presence of proteasome inhibition and analyzed by SDS polyacrylamide gel electrophoresis (PAGE)[32]. We observed a pronounced ladder of ubiquitylated pHA-*Pb*CSP^{WT} in cells upon proteasome inhibition (Fig. 1b), indicating the ability of the host UPS machinery to ubiquitylate *Pb* CSP in the absence of other parasite proteins. Interestingly, the total cell lysate did not show an increase in CSP expression in HepG2 and HEK 293 T cells treated with proteasome inhibitors when compared to lanes without MG132 treatment (Fig. 1 and Supplementary Fig. 1c and 1d), suggesting that only a small fraction of ubiquitylated CSP is degraded by the 26S proteasome.

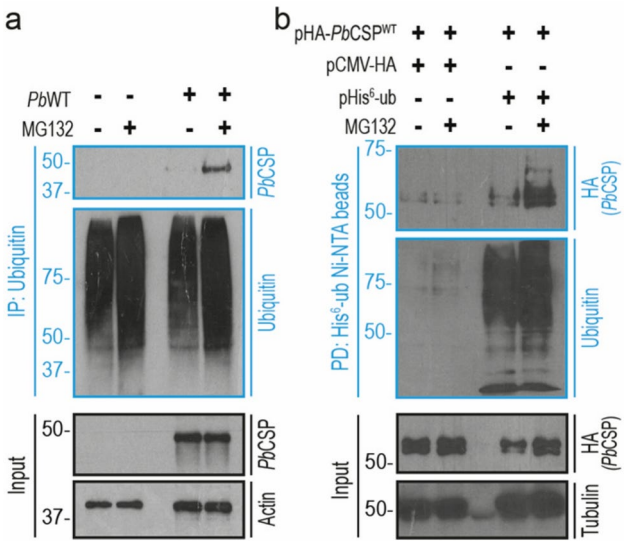

Fig. 1. *Pb* CSP is ubiquitylated by mammalian cells. (a) HepG2 cells pretreated or not with proteasome inhibitor MG132 were infected with *P. berghei* wild type (*Pb*WT) sporozoites. At 4 h post-infection (hpi), whole cell lysate was harvested, lysed, and subjected to immunoprecipitation (IP) using an anti-ubiquitin antibody. The immunoprecipitates and the total cell lysate input before IP were analyzed by western blotting, using anti-*Pb*CSP (3D11), anti-ubiquitin, and anti-actin antibodies, as indicated. Illustrative image of 3 independent experiments. (b) HEK 293 T cells were transiently co-transfected with the indicated plasmids (on top) and treated with MG132 for 8 h. When required, an empty vector (pCMV-HA) was used to normalize the total DNA amount. At 48 h post-transfection, cells were harvested, lysed, and subjected to Ni–NTA beads pull-down (PD) of histidine-tagged ubiquitin. Ubiquitylated CSP was detected using anti-HA antibody by western blot. Anti-ubiquitin and anti-actin antibodies were also used as indicated Illustrative image of 4 independent experiments. Uncropped blots of Fig. 1a and Fig. 1b are shown in Supplementary Information 1 and 2, respectively.

Mammalian E3 Cullin RING Ligases can mediate *Pb* CSP ubiquitylation

The specificity of the ubiquitylation enzymes in the cascade and the recognition of target proteins relies on the catalytic action of E3 ubiquitin ligases, which facilitate the transfer of mono- or polyubiquitin chains to the lysine (K) residues in the substrate protein. Among these, the E3 Cullin RING ligases (CRLs) are the largest and most studied family of E3 ligases[34,35]. The CRLs are multi-subunit complexes, that are regulated via neddylation, sharing a similar core architecture, with each specific Cullin (CUL) protein acting as a molecular scaffold[36]. To determine the impact of CRLs in *Pb* CSP ubiquitylation during hepatocyte infection, we repeated the experimental set-up of Fig. 1a and used a CRL inhibitor—MLN4924[37], that inhibits neddylation, and hence the activity of CRLs. To this end, HepG2 cells were co-treated with MG132 and MLN4924, followed by infection with *Pb*WT sporozoites. At 4 hpi, whole cell lysates were subjected to immunoprecipitation for total endogenous ubiquitin, and eluted proteins were analyzed by immunoblotting. Our results showed that the co-treatment with MG132 and MLN4924 decreased CSP ubiquitylation, as it diminished the expected amount of CSP co-immunoprecipitated with ubiquitin (Fig. 2a). This observation cannot be attributed to an unspecific impact of MLN4924 and MG132 co-treatment on the parasite itself as we do not observe any deficit in sporozoite traversal, invasion, and establishment in hepatocytes in the presence of these inhibitors (Supplementary Fig. 2a, b, and c, respectively). Altogether this suggests that host CRLs are involved in the ubiquitylation of *Pb* CSP.

There are eight classes of CRL proteins in mammals, with a CUL protein acting as a central scaffold. Cullins bind to an adaptor protein and a substrate receptor protein on one end, and an E2 protein on the other. To further understand the involvement of E3 CRL complexes in *Pb* CSP ubiquitylation, HEK 293 T cells were co-transfected with plasmids expressing different Cullins, pHA-*Pb*CSP^{WT}, and pHis^{6}-ub, in the presence of proteasome inhibition. As in Fig. 1b, ubiquitylated CSP was purified under denaturing conditions via Ni–NTA agarose beads and analyzed by immunoblotting. The expression of each Cullin led to a notable increase in the ladder of ubiquitylated *Pb* CSP (Supplementary Fig. 2d), thus we selected the most abundant CUL and best-characterized E3 CRL complex—the Skp1-Cullin-F-box[38] (also known as SCF or CRL1)[39], as a tool to further investigate the role of *Pb* CSP ubiquitylation during liver stage infection.

To this end, we first validated the interaction between host CUL1 and *Pb* CSP. HEK 293 T cells were transfected with pHA-*Pb*CSP^{WT} either by itself or together with pcDNA3-CUL1-Myc (to overexpress CUL1) followed by immunoprecipitation of CUL1, in the presence of MG132. We found that *Pb* CSP is co-immunoprecipitated with CUL1, even without CUL1 overexpression (Fig. 2b, lane 3). This result was further validated by the co-immunoprecipitation of *Pb* CSP with CUL1 from *Pb*WT-infected HepG2 cells, at 4hpi (Fig. 2c). In infected HepG2 cells co-treated with MG132 and MLN4924, we did not observe an alteration in the abundance of total *Pb* CSP (Supplementary Fig. 2e). Similar results were obtained in HEK 293 T cells co-transfected with pHA-*Pb*CSP^{WT} and pcDNA3-CUL1-Myc (Supplementary Fig. 2f.). This suggests that only a small fraction of *Pb* CSP is

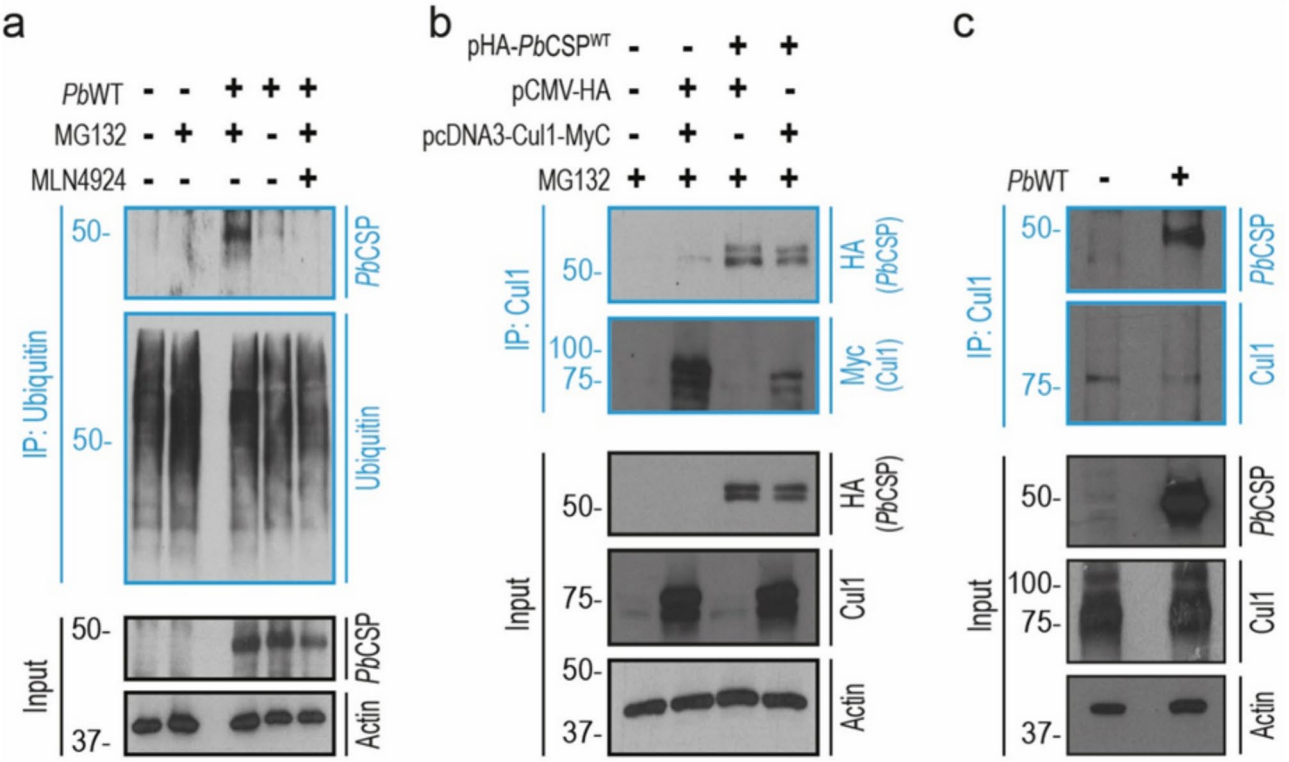

Fig. 2. Host Cullin 1 interacts with *Pb*CSP during hepatocyte infection. (**a**) HepG2 cells pretreated or not, with the proteasome inhibitor MG132, and/or MLN4924 were infected with *P. berghei* wild type (*Pb*WT) sporozoites, and total cell lysates subjected to immunoprecipitation (IP) with anti-ubiquitin antibody, at 4 h post-infection (hpi). IP elute and total lysate input before IP were analyzed by immunoblotting using anti-*Pb*CSP (3D11), anti-ubiquitin and anti-actin antibodies. Illustrative image of 2 independent experiments. (**b**) HEK293T cells transiently co-transfected with the indicated plasmids (on top) and treated with MG132. When required, an empty vector (pCMV-HA) was used to normalize the total DNA amount. At 48 h post-transfection (and 8 h of MG132 treatment) cells were harvested, lysed, and subjected to immunoprecipitation (IP) using an anti-CUL1 antibody. Purified elute and input before IP were analyzed by immunoblotting using the indicated antibodies. Illustrative image of 2 independent experiments. (**c**) HepG2 cells were infected with *Pb*WT sporozoites, and lysates were subjected to an IP with an anti-CUL1 antibody, at 4 h post-infection (hpi). IP elute and input before IP were analyzed by immunoblotting using anti-*Pb*CSP, anti-CUL1, and anti-actin antibodies. Illustrative image of 2 independent experiments. Uncropped blots of Fig. 2a, 2b, and 2c are shown in Supplementary Information 3, 4, and 5, respectively.

degraded by host UPS within infected hepatocytes. To control for unspecific binding in the immunoprecipitation experiments, lysates of infected HepG2 cells were incubated with beads not coated with anti-CUL1 primary antibody (Supplementary Fig. 3). Together, these findings show that CUL1 interacts with *Pb* CSP and possibly ubiquitylates it. Furthermore, in agreement with the previous data (Supplementary Fig. 1c and 1d), MG132 treatment and CUL1 overexpression did not alter CSP abundance in transfected cells (Supplementary Fig. 2e and 2f.), suggesting that only a small fraction of CSP is degraded by the host UPS.

Since we show that CUL1 and *Pb* CSP interact in an infection context, we next questioned whether the loss of CUL1 could affect *Pb* infection. As knockout of E3-CRL proteins causes early embryonic lethality in mice[40] we decided to use small-interfering RNA (siRNA) to knock down CUL1 protein levels ex vivo (Supplementary Fig. 4a). Primary hepatocytes from C57BL/6 J mice were transfected with si-CUL1 or si-CT (scrambled control) (Supplementary Fig. 4b) and infected with *Pb*WT sporozoites 24 h after transfection. Parasite load was assessed by qPCR at 4 hpi. We did not observe any reduction in parasite load (Supplementary Fig. 4c), indicating that CUL1 does not affect the early stages of *Plasmodium* liver infection.

The K252 and K258 moieties of the *Pb* CSP C-terminal region are key ubiquitylation targets

Having established that mammalian liver cells can ubiquitylate *Pb* CSP, we sought to determine the specific region/s and K residue/s involved in its ubiquitylation.

Plasmodium CSP is a glycosylphosphatidylinositol (GPI)-anchored membrane protein[41], with common structural features among the various *Plasmodium* species[42], including (i) an N-terminal signal peptide sequence, (ii) a conserved region I (RI), (iii) a tandemly species-specific central domain composed of amino acids repeats, (iv) and a C-terminal cell-adhesion domain (type I thrombospondin repeat)[42,43].

To identify the putative amino acid residues ubiquitylated in *Pb* CSP, we designed three mutants of the previously used HA-p*Pb*CSP^{WT} construct, in which all the K moieties of either the N-terminal, the RI, or the C-terminal regions were independently mutated into arginines (R) (pHA-*Pb*CSP$^{K\text{-}NT\text{-}R}$, pHA-*Pb*CSP$^{K\text{-}RI\text{-}R}$ and pHA-*Pb*CSP$^{K\text{-}CT\text{-}R}$, respectively) (Fig. 3a). HEK 293 T cells were co-transfected with pHis^6-Ub and either the control p*Pb*CSP^{WT} or one of the mutated constructs, subjected to MG132 treatment, followed by ubiquitin pull-down with Ni–NTA beads. The total CSP polyubiquitylation in the pHA-*Pb*CSP$^{K\text{-}CT\text{-}R}$ mutant appeared reduced relative to pHA-*Pb*CSP^{WT} and the other mutants (Fig. 3b). This hinted towards the C-terminal K moiety(ies) as potential sites involved in CSP ubiquitin-tagging.

To identify the position of the C-terminal lysine residues, we used CUL1 overexpression as a tool to increase *Pb* CSP ubiquitylation and coupled it to CSP affinity purification by immunoprecipitation with mass spectrometry analysis[44,45]. Briefly, three 10 cm Petri dishes with HEK 293 T cells were co-transfected with plasmids expressing pHA-*Pb*CSP^{WT}, pHis^6-ub, and pcDNA3-CUL1-Myc. At 40 h after transfection (and 8 h of MG132 treatment), the total lysate of each dish was used to immunoprecipitate CSP using three different approaches: (i) anti-HA magnetic IP/Co-IP beads, (ii) Protein A/G-plus agarose beads cross-linked to anti-HA high-affinity rat mAb (iii) and Protein A/G-plus agarose beads cross-linked to anti-3D11 mAb antibodies. With this heterologous approach, we excluded potential contributions of other parasite proteins, since eluted proteins are from mammalian cells overexpressing CSP, and not from cells infected with *Plasmodium* sporozoites.

Purification products were subsequently sent to the Centre for Genomic Regulation (in Barcelona, Spain) for further digestion with trypsin, enrichment of ubiquitylated peptides using di-glycine (DiGLY) remnant (which is attached to the ubiquitylated residues following the digestion of ubiquitin by trypsin[46]), and mass spectrometry (MS) analysis. MS runs identified a total of 21 peptides mapped to the *Pb* ANKA CSP sequence,

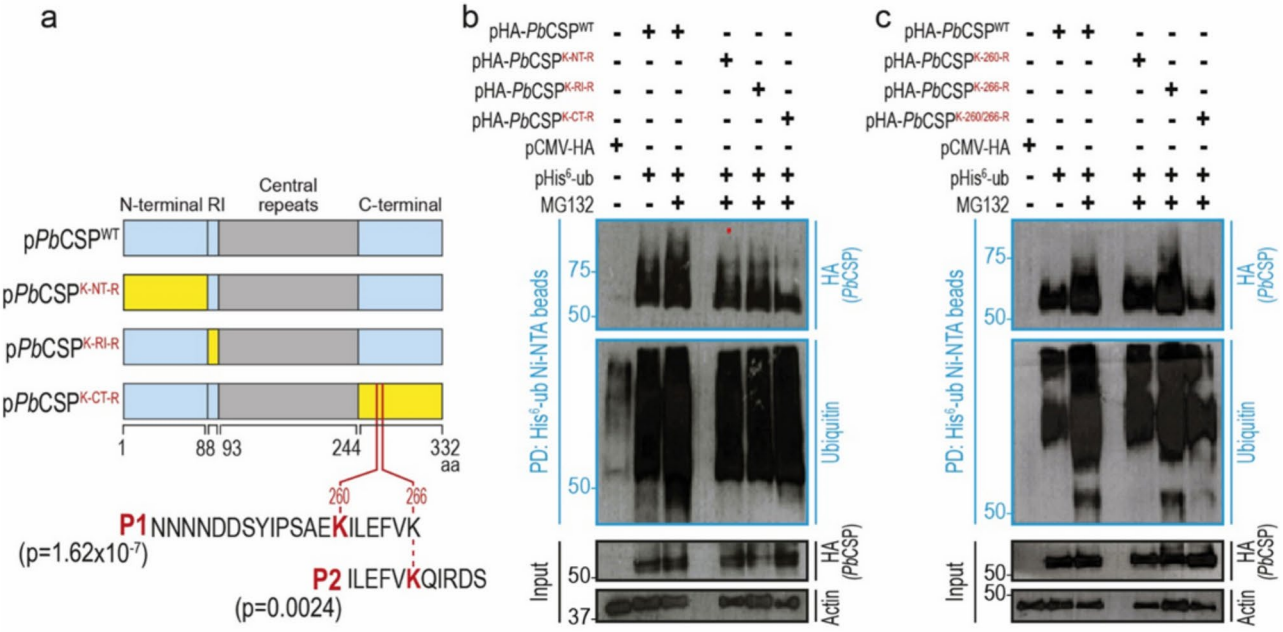

Fig. 3. *Pb* CSP is ubiquitylated at K-252 and K-258 moieties of the C-terminal region. (**a**) Schematic representation of wild-type *Pb* ANKA CSP (p*Pb*CSP^{WT}) and mutant CSP (p*Pb*CSP$^{K\text{-}NT\text{-}R}$, p*Pb*CSP$^{K\text{-}RI\text{-}R}$, p*Pb*CSP$^{K\text{-}CT\text{-}R}$) protein. Blue rectangles represent unmutated CSP regions and yellow rectangles represent regions with all lysine (K) residues mutated into arginine (R). P1 represents the peptide identified by mass spectrometry containing diGLY modifications, using the anti-HA magnetic IP/Co-IP beads, and P2 to the peptide identified using Protein A/G-plus agarose beads cross-linked to anti-HA high-affinity rat mAb. p = confidence measure on the identified peptide expected value. (**b**) Ni–NTA pull-down (PD) of histidine-tagged ubiquitin from lysates of HEK 293 T cells co-expressing pHis6-ub and either the wild-type or the mutant CSP versions for 48 h, and treated with MG132 for 8 h before PD. PD proteins and total cell lysate input before PD were obtained 48 h post-transfection and analyzed by immunoblotting using anti-HA (for *Pb*CSP), anti-ubiquitin, and anti-actin antibodies, as indicated. Illustrative image of 4 independent experiments. (**c**) Ni–NTA PD of histidine-tagged ubiquitin from HEK 293 T cell lysates co-expressing pHis6-ub and mutant versions of p*Pb*CSP^{WT} constructs, with K14 of the Peptide 1 and K6 of Peptide 2 identified by mass spectrometry with a diGLY modification, replaced by arginine (pHA-*Pb*CSP$^{K\text{-}260\text{-}R}$, pHA-*Pb*CSP$^{K\text{-}266\text{-}R}$, and pHA-*Pb*CSP$^{K\text{-}260/266\text{-}R}$). PD proteins and total cell lysate input before PD were obtained 48 h post-transfection (and 8 h of MG132 treatment) and analyzed by immunoblotting using anti-HA (for CSP), anti-ubiquitin, and anti-actin antibodies. Illustrative image of 4 independent experiments. NT = N-terminal, RI = Region I, CT = C-terminal. For Fig. 3b and 3c, an empty vector (pCMV-HA) was used to normalize the total DNA amount. Uncropped blots of Fig. 3b, and 3c are shown in Supplementary Information 8 and 9, respectively.

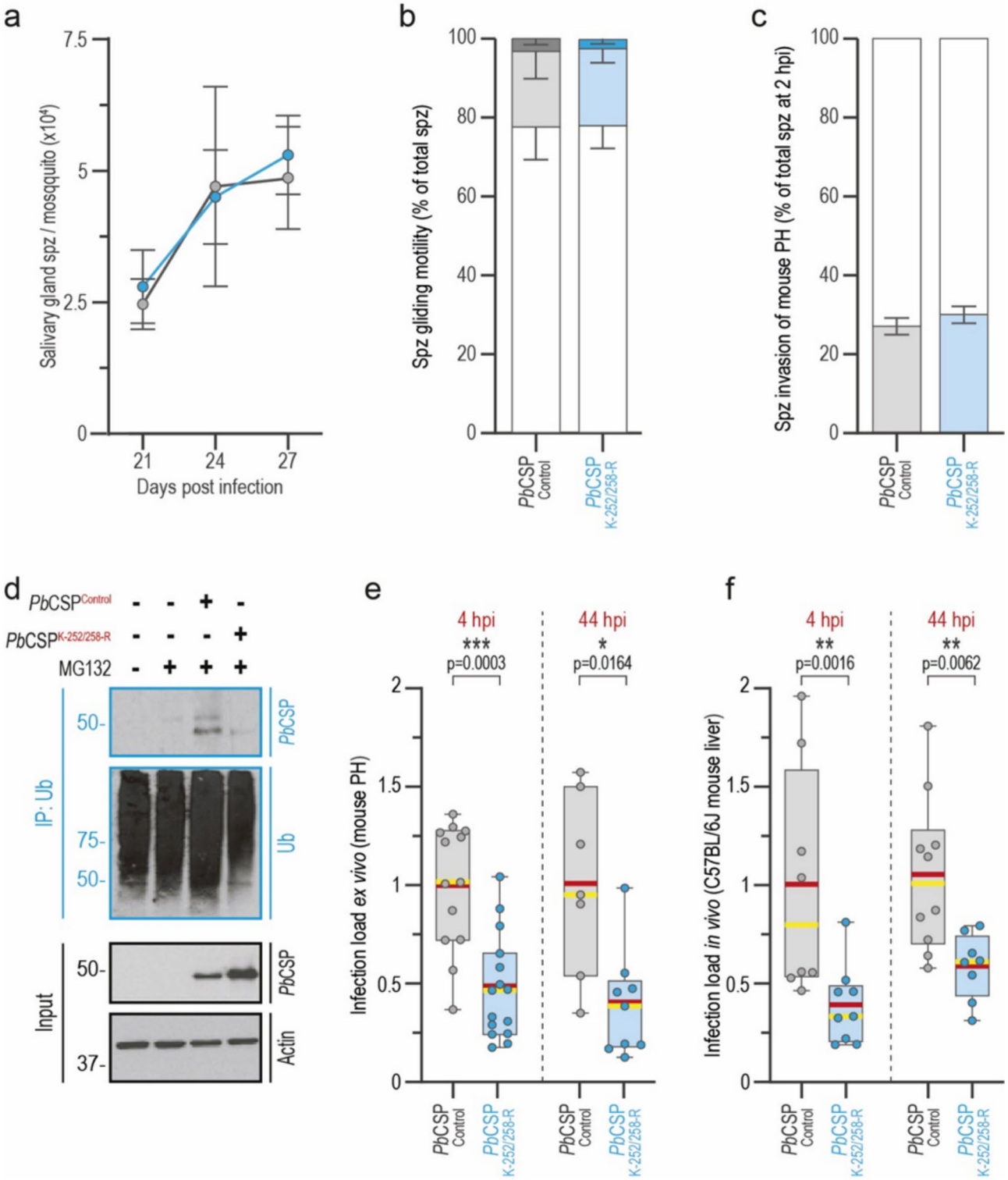

two of which had a DiGLY modification (Supplementary Table 1). One peptide (P1) was identified using the anti-HA magnetic IP/Co-IP beads and the other peptide (P2) using Protein A/G-plus agarose beads cross-linked to anti-HA high-affinity rat mAb (peptides highlighted in blue in Supplementary Table 1). The other modifications identified were carbamidomethylation of cysteine and oxidation of methionine. Since P2 is also present within P1 (Fig. 3a), we performed a BLAST to search for proteins with the identified peptide and whose matched values are statistically significant (below 0.001). *Pb* CSP was identified with at least 95% confidence, therefore excluding that P1 and P2 could come from contaminant proteins.

To further validate MS results, we mutated the K moieties identified in P1 and P2 to R residues on the pHA-*Pb*CSP^{WT} construct, individually or in combination, generating three variants- pHA-*Pb*CSP$^{K\text{-}260\text{-}R}$, pHA-*Pb*CSP$^{K\text{-}266\text{-}R}$, and pHA-*Pb*CSP$^{K\text{-}260/266\text{-}R}$. We next transfected HEK 293 T cells with these constructs and with pHis^{6}-Ub and treated them with MG132. Ni–NTA pull-down of ubiquitylated proteins indicated a reduction in

◀**Fig. 4**. CSP ubiquitylation impacts *Pb* early liver stage infection. (a) The number of salivary glands sporozoites in mosquitos infected with *Pb*CSP^{Control} (gray) or *Pb*CSP$^{K\text{-}252/258\text{-}R}$ (cyan) parasites, was assessed by salivary gland dissection and sporozoite counting at different days post-infection. Results are shown as mean ± SEM of at least 3 independent experiments, with a minimum of 150 infected mosquitoes analyzed per parasite line per time. (**b**) Gliding motility of *Pb*CSP^{Control} (shades of gray) and *Pb*CSP$^{K\text{-}252/258\text{-}R}$ (shades of cyan) sporozoites. Sporozoites were scored as having 0 (white bars), between 1–5 (light grey/cyan bars), between 6–10 (dark grey/cyan bars) and > 11 trails (black bars). Results of 3 independent experiments. A total of 479 *Pb*CSP^{Control} and 901 *Pb*CSP$^{K\text{-}252/258\text{-}R}$ sporozoites were scored. (**c**) Percentage of total intracellular and extracellular sporozoites (*Pb*CSP^{control}: gray; *Pb*CSP$^{K\text{-}252/258\text{-}R}$: cyan) observed by IFA of infected mouse primary hepatocytes (PH), at 2hpi. Results of 2 independent experiments. A total number of 1366 *Pb*CSP^{control} sporozoites and 1900 *Pb*CSP$^{K\text{-}252/258\text{-}R}$ sporozoites were analyzed. (**d**) HepG2 cells pretreated with proteasome inhibitor MG132 were infected with either *Pb*CSP^{control} or *Pb*CSP$^{K\text{-}252/258\text{-}R}$ sporozoites. At 4 h post-infection (hpi), whole cell lysate was harvested, lysed, and subjected to immunoprecipitation (IP) using an anti-ubiquitin antibody. Immunoprecipitates and lysate input before IP were analyzed by western blotting using anti-CSP (3D11), anti-ubiquitin, and anti-actin antibodies. Illustrative image of 2 experiments. (**e**) Liver load of cultured primary hepatocytes from C57BL/6 J mice infected with *Pb*CSP^{control} (gray) or *Pb*CSP$^{K\text{-}252/258\text{-}R}$ (cyan) sporozoites, assessed by qPCR at 4 and 44 hpi. Experiments were done with at least 3 technical replicates per parasite line and per time-point. (**f**) Liver infection load of C57BL/6 J mice infected with *Pb*CSP^{control} (gray) or *Pb*CSP$^{K\text{-}252/258\text{-}R}$ (cyan) sporozoites assessed by qPCR at 4 and 44 hpi. Results are shown as boxplots (min-to-max) of 2 independent experiments, with at least 4 technical replicates per parasite line and per time-point. In Figs. 4b and 4c results are shown as bar graphs. In Figs. 4e, and 4f, results are shown as boxplots (min-to-max). The red bar indicates the mean and the yellow bar indicates the median. The Two-tailed Mann–Whitney U test was applied for *p*-values, ** $p < 0.005$; ***$p < 0.001$. Uncropped blots of Fig. 4d are shown in Supplementary Information 11.

Pb CSP ubiquitylation ladder in cells expressing double mutant HA-p*Pb*CSP$^{K\text{-}260/266\text{-}R}$, in comparison with cells transfected with either the control HA-p*Pb*CSP^{WT} construct or the single mutant constructs (Fig. 3c). However, as we did not observe a total loss of CSP ubiquitylation in cells transfected with HA-p*Pb*CSP$^{K\text{-}260/266\text{-}R}$, and we previously showed that each E3 CRL individually increased *Pb* CSP ubiquitylation (Supplementary Fig. 2d), these findings suggest that additional CSP lysine residues may be targeted for ubiquitylation.

Host-mediated ubiquitylation at *Pb* CSP K252 and K258 ensures parasite survival in early liver stages

We then set out to explore whether the lack of *Pb* CSP ubiquitylation at both lysine residues would impact *Plasmodium* liver stage infection as CSP activity is known to be essential for sporozoite formation[5]. For this purpose, we used *Plasmodium berghei* NK65 strains (parental line for genetic modifications, also used by others to study mutation in *Pb* CSP[10,47]) and identified the lysine residues 252 and 258 in the NK65 strain that corresponds to K260 and K266 in the ANKA strain. A mapping illustrating the alignment of CSP sequences between ANKA and NK65 strains is provided in the Supplementary Fig. 5a. To ensure clarity, from this moment on, all residue positions referenced in this study correspond to the NK65 sequence unless explicitly stated otherwise. Next, we developed a *Pb* transgenic parasite line—*Pb*CSP$^{K\text{-}252/258\text{-}R}$ – with the two identified ubiquitylated lysines mutated into arginines. Mutant parasites were obtained by double homologous recombination to replace the endogenous CSP coding sequence locus from GFP expressing *Pb*ANKA parasite line-507cl[48] (GFP-*Pb*WT$^{(ANKA)}$) with the mutated CSP gene from *Pb*NK65. In parallel, a control parasite line was generated – *Pb*CSP^{Control} – where the WT *Pb*NK65 CSP coding sequence replaced the native *Pb*ANKA CSP gene[6] (Supplementary Fig. 5b).

Both transgenic parasite lines were viable and generated comparable numbers of salivary gland sporozoites (Fig. 4a). Additionally, both parasite lines exhibited an identical number of trails generated by sporozoites (a measurement of sporozoite gliding motility) (Fig. 4b). Next, we addressed whether these sporozoites had the same invasion capacity. To determine the ratio between sporozoites that invaded hepatocytes and that remained outside of the cells, we employed a differential staining strategy that utilizes sequential CSP detection before and post permeabilization[49]. Interestingly, no differences were observed at 2 hpi (Fig. 4c and Supplementary Fig. 5c). Together, these findings indicate that the K252/K258R substitution on *Pb* CSP did not affect parasite sporogony, gliding, and invasion capabilities.

To validate the in vitro findings on the impact of these K moieties on *Pb* CSP ubiquitylation, we replicated the experimental set-up of Fig. 1a, in the context of infection. HepG2 cells were infected with either *Pb*CSP^{Control} or *Pb*CSP$^{K\text{-}252/258\text{-}R}$ sporozoites in the presence of MG132 treatment. At 4 hpi cells were harvested and total ubiquitin was immunoprecipitated. Immunoblotting analysis of the purified eluted proteins showed a striking reduction in the levels of *Pb* CSP co-immunoprecipitating with endogenous ubiquitin in cells infected with *Pb*CSP$^{K\text{-}252/258\text{-}R}$ relative to *Pb*CSP^{Control} sporozoites (Fig. 4d).

Next, we isolated and cultured primary hepatocytes (PH) from C57BL/6 J mice and infected with *Pb*CSP$^{K\text{-}252/258\text{-}R}$ freshly dissected sporozoites to assess infection load (infection of ex vivo cultured primary hepatocytes), at 4 and 44 hpi, by qPCR. A significant reduction in infection load was observed at 4 and 44 hpi ($p = 0.0003$ and $p = 0.0164$, respectively) in transgenic *Pb*CSP$^{K\text{-}252/258\text{-}R}$ parasites when compared to *Pb*CSP^{Control} (Fig. 4e). This decreased load was not due to impaired intrahepatic parasite development, as both lines showed parasites with comparable sizes (at 44 hpi) (Supplementary Fig. 5d), suggesting that upon successful infection, parasite development in primary hepatocytes is not compromised. We also assessed the number of infected cells by immunofluorescence (IFA) at 4 hpi and 44 hpi[49], which similarly to our qPCR data showed a decrease in the

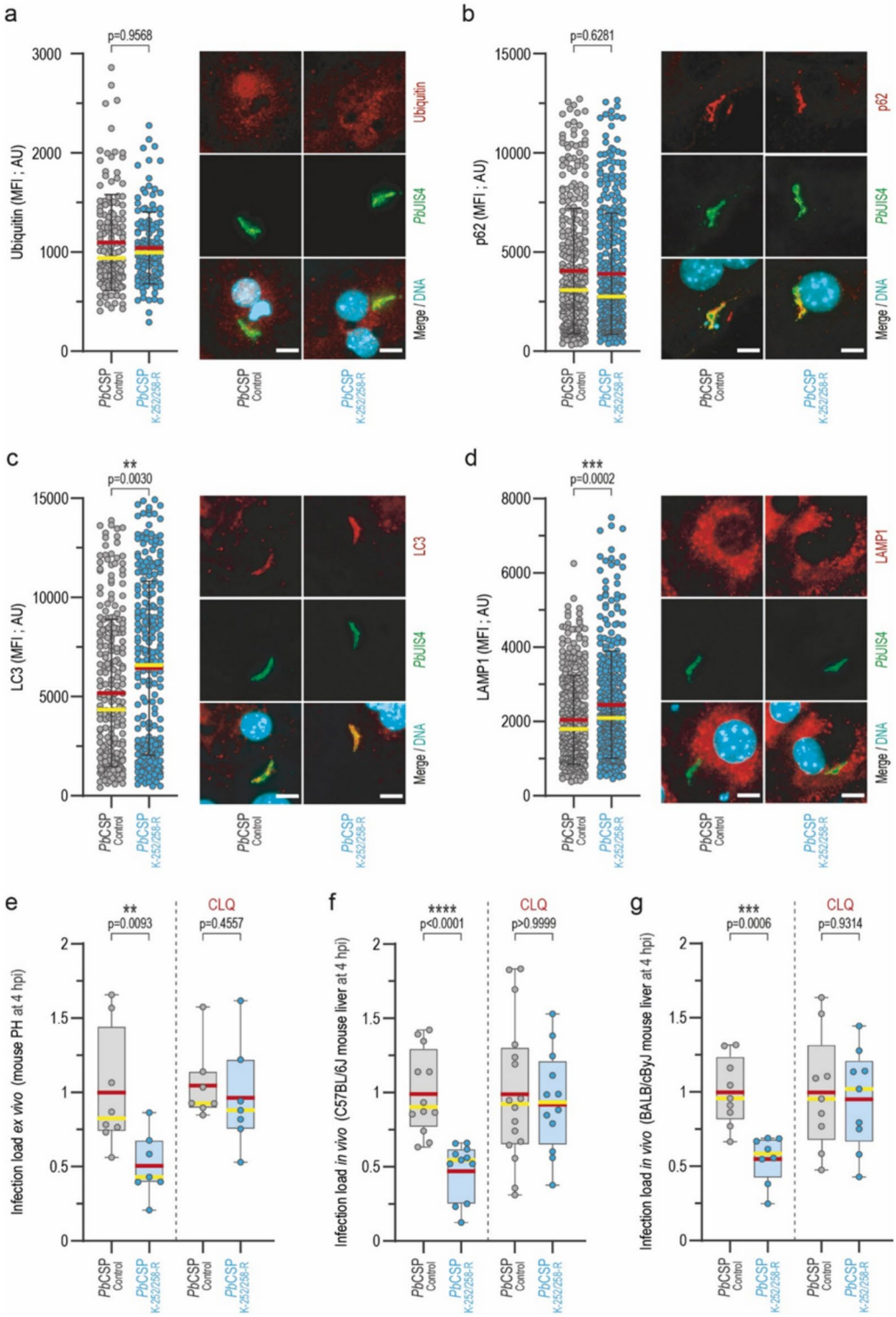

number of *Pb*CSP$^{K\text{-}252/258\text{-}R}$ infected cells (Supplementary Fig. 5e), supporting that CSP ubiquitylation at K252 and K258 ensures a successful primary hepatocyte infection.

To validate our findings in vivo, C57BL/6 J mice were infected with *Pb*CSP^{Control} or *Pb*CSP$^{K\text{-}252/258\text{-}R}$ sporozoites, and hepatic infection load was assessed by qPCR at 4 hpi and 44 hpi. At both developmental time points, hepatic infection load with *Pb*CSP$^{K\text{-}252\text{-}/258\text{-}R}$ parasite was approximately half of the control (*Pb*CSP^{Control})(Fig. 4f). Similarly, our results showed a significant decrease in *Pb*CSP$^{K\text{-}252/258\text{-}R}$ hepatic infection load at 4 hpi and 44 hpi ($p = 0.0029$ and $p = 0.0111$, respectively) in livers of infected BALB/cByJ mice (Supplementary Fig. 5f.).

Collectively, our ex vivo and in vivo data shows that *Pb*CSP ubiquitylation at the K252 and K258 residues of its C-terminus is necessary for the establishment of a productive liver stage infection.

◀**Fig. 5**. Loss of *Pb* CSP ubiquitylation promotes parasite early elimination by host autophagy. (**a**) Representative micrographs of early *Pb*CSP^{control} (gray) or *Pb*CSP$^{K\text{-}252/258\text{-}R}$ (cyan) EEFs used to measure the mean fluorescence intensity (MFI) of ubiquitin in infected PH from C57BL/6 J mice, at 4 hpi. Results are shown as dot-plots (mean ± SEM) of 2 independent experiments with a total of 164 EEFs for *Pb*CSP^{control} and 146 EEFs for *Pb*CSP$^{K\text{-}252/258\text{-}R}$. Red bar indicates the mean; yellow bar indicates the median. Two-tailed Mann–Whitney U test was applied for p-values **, $p < 0.005$; ***, $p < 0.001$. Parasites were stained with ubiquitin (red), PbUIS4 (green) and Hoechst (cyan). Scale bar: 10 µm. (**b**) Same as in Fig. 5a but for p62. Results are shown as dot-plots (mean ± SEM) of 3 independent experiments with a total of 329 EEFs for *Pb*CSP^{control}, and 342 EEFs for *Pb*CSP$^{K\text{-}252/258\text{-}R}$. Red bar indicates the mean, yellow bar indicates the median. Two-tailed Mann–Whitney U test was applied for p-values **, $p < 0.005$; ***, $p < 0.001$. Parasites were stained with p62 (red), *Pb*UIS4 (green) and Hoechst (cyan). Scale bar: 10 µm. (**c**) Same as in Fig. 5a but for LC3. Results are shown as dot-plots (mean ± SEM) of 3 independent experiments with a total of 113 EEFs for *Pb*CSP^{control}, and 106 EEFs for *Pb*CSP$^{K\text{-}252/258\text{-}R}$. Red bar indicates the mean, yellow bar indicates the median. Comparison of the median intensity signal between the *Pb*CSP^{control} or *Pb*CSP$^{K\text{-}252/258\text{-}R}$ parasite lines, identified LC3 signal ca. 42% more intense on the mutant parasites relative to the control parasites. Two-tailed Mann–Whitney U test was applied for p-values **, $p < 0.005$; ***, $p < 0.001$. Parasites were stained with LC3 (red), *Pb*UIS4 (green) and Hoechst (cyan). Scale bar: 10 µm. (**d**) Same as in Fig. 5a but for LAMP1. Results are shown as dot-plots (mean ± SEM) of 3 independent experiments with a total of 360 EEFs for *Pb*CSP^{control}, and 355 EFs for *Pb*CSP$^{K\text{-}252/258\text{-}R}$. Red bar indicates the mean, yellow bar indicates the median. Comparison of the median intensity signal between the *Pb*CSP^{control} or *Pb*CSP$^{K\text{-}252/258\text{-}R}$ parasite lines, identified Lamp1 signal ca. 14% more intense on the mutant parasites relative to that on control parasites. Two-tailed Mann–Whitney U test was applied for p-values **, $p < 0.005$; ***, $p < 0.001$. Parasites were stained with LAMP1 (red), *Pb*UIS4 (green) and Hoechst (cyan). Scale bar: 10 µm. (**e**) PH from C57BL/6 J mice were pretreated or not with Chloroquine and infected with *Pb*CSP^{control} (gray) or *Pb*CSP$^{K\text{-}252/258\text{-}R}$ (cyan) sporozoites. Infection load was assessed by qPCR at 4 hpi. Results are shown as boxplots (min-to-max) of 2 independent experiments in quadruplicates per parasite line per experiment. Red bar indicates the mean, yellow bar indicates the median. Two-tailed Mann–Whitney U test was applied for p-values **, $p < 0.005$; ***, $p < 0.001$. (**f**) Liver infection load of C57BL/6 J mice infected with *Pb*CSP^{control} (gray) or *Pb*CSP$^{K\text{-}252/258\text{-}R}$ (cyan) treated or not with Chloroquine at 24 and 2 h before infection, was assessed by qPCR at 4 hpi. Results are shown as boxplots (min-to-max) of 3 independent experiments. In total 13 mice for mock treatment and 17 mice for Chloroquine treatment, were scored. Red bar indicates the mean, yellow bar indicates the median. Two-tailed Mann–Whitney U test was applied for p-values **, $p < 0.005$; ***, $p < 0.001$. (**g**) Same as in Fig. 5f but in BALB/c mice. Results are shown as boxplots (min-to-max). In total 9 mice for mock treatment and 10 mice for Chloroquine treatment, were scored. Red bar indicates the mean, yellow bar indicates the median. Two-tailed Mann–Whitney U test was applied for p-values **, $p < 0.005$; ***, $p < 0.001$.

Lack of appropriate *Pb* CSP ubiquitylation makes the parasite susceptible to targeting by host autophagic machinery

It is well established that autophagy is one of the earliest mechanisms for *Plasmodium* liver stage elimination [22–24] and that ubiquitylation can regulate many steps of autophagy and cell death pathways[50,51]. Having observed that a significant proportion of *Pb*CSP$^{K\text{-}252/258\text{-}R}$ sporozoites are eliminated earlier in hepatic infection, we hypothesized that *Pb* CSP ubiquitylation could be involved in the regulation of a cell-autonomous mechanism of parasite clearance such as autophagy.

Using the established ex vivo model and IFA, we started by analyzing the overall expression of ubiquitin and its intracellular localization within mouse primary hepatocytes infected with either *Pb*CSP^{Control} or *Pb*CSP$^{K\text{-}252/258\text{-}R}$ sporozoites, at 4 hpi. We observed no differences in the fluorescence intensity and localization of ubiquitin at the parasitophorous vacuole membrane (PVM) of either parasite line (Fig. 5a), suggesting that the overall PVM ubiquitylation is not affected in *Pb*CSP$^{K\text{-}252/258\text{-}R}$ parasites.

Similarly, no difference could be observed by IFA in the fluorescence intensity and localization of p62 of either parasite strain in infected mouse primary hepatocytes (Fig. 5b). This observation suggests that p62 is not responsible for *Pb*CSP$^{K\text{-}252/258\text{-}R}$ parasite clearance in early infection.

Next, we compared the fluorescence intensity and localization patterns of key autophagy and lysosome markers- the microtubule-associated protein 1 light chain 3 (LC3) and the lysosomal-associated membrane protein 1 (LAMP1). Our results showed that *Pb*CSP$^{K\text{-}252/258\text{-}R}$ parasites had significantly increased levels of LC3 ($p = 0.0030$) and LAMP1 ($p = 0.0002$) relative to *Pb*CSP^{Control} parasites in infected hepatocytes, at 4 hpi (Fig. 5c and d, respectively), implying that the mutations at the K252 and K258 residues of *Pb* CSP render parasites more susceptible to be targeted by ubiquitin-independent but LC3-dependent host autophagy machinery.

To validate the role of host autophagy in the reduction of *Pb*CSP$^{K\text{-}252/258\text{-}R}$ parasite numbers, we tested whether chloroquine (CLQ), a well-known autophagy inibithor[52], would rescue mutant parasite elimination. Mouse primary hepatocytes were pre-incubated with CLQ and infected with *Pb*CSP^{Control} or *Pb*CSP$^{K\text{-}252/258\text{-}R}$ sporozoites. Infection load was obtained at 4 hpi by qPCR (Fig. 5e). Our results indicate that inhibition of host lysosome-autophagosome interaction by CLQ rescued the *Pb*CSP$^{K\text{-}252/258\text{-}R}$ phenotype, restoring liver stage infection levels to the ones observed for control parasites. Importantly, these observations were further confirmed in vivo, using both C57BL/6 J and BALB/cByJ mice treated by intraperitoneal injection of CLQ 4 h and 28 h prior to infection (Fig. 5f and g, respectively). Collectively, these results suggest that *Pb* CSP ubiquitylation at its C-terminal residues, K252 and K258, are key to avoid parasite elimination by lysosomes, in early stages of hepatocyte invasion.

Discussion

Ubiquitylation is crucial for maintaining cellular homeostasis, including the recognition and clearance of pathogens, via proteasomal degradation and/or autophagy. In this study, we reveal a novel link between the ubiquitylation of the major sporozoite surface protein, CSP, and inhibition of liver stage parasite elimination during early hepatic infection. Based on dogma, we anticipated that CSP ubiquitylation would lead to parasite clearance through canonical proteasomal degradation. Contrary to expectations, we discovered that ubiquitylation of C-terminal CSP at lysine residues K252 and K258, is essential for successful *Plasmodium* hepatocyte invasion. By preventing CSP ubiquitination at these moieties, we observed a marked decrease in the establishment of *Plasmodium* infection in primary hepatocytes.

Previous studies identified the glycosylation of CSP at the C-terminal region (Thr337) as a key PTM, essential for mosquito midgut colonization and salivary gland invasion by *P. falciparum* sporozoites[21,53,54] and that CSP proteolytic processing was crucial for invasion of hepatocytes[10]. Our study highlights a novel function for CSP ubiquitylation, as a relevant PTM for a successful liver stage infection. We observed that *Pb*CSP$^{K\text{-}252/258\text{-}R}$ sporozoites were present in normal numbers in female *Anopheles* mosquitos and retained their ability to glide and invade hepatocytes, indicating that these residues are not required for sporogony, migration, or hepatocyte invasion. Instead, their ubiquitylation appears to be relevant for parasite survival within hepatocytes.

The phenotype we present here aligns with previous studies, which showed that impairments in parasite elimination during hepatic infection are due to the ubiquitylation of host autophagy-related proteins in hepatocytes by the host E3 ligase NEDD4[55] and degradation of host LC3B[56]. In the future, it would be interesting to explore whether CSP ubiquitylation regulates the degradation of host autophagy-related proteins.

This study aimed to uncover the function of *Pb* CSP ubiquitylation during early liver stage infection. To better dissect the host ubiquitylation machinery, we used CUL1 to artificially increase CSP ubiquitylation levels, demonstrating that the host ubiquitin–proteasome machinery interacts with CSP. We observed a reduced parasite load in primary hepatocytes infected with *Pb*CSP$^{K\text{-}252\ /258\text{-}R}$ at 4 hpi and a drastic decrease in *Pb* CSP ubiquitylation in cells infected with *Pb*CSP$^{K\text{-}252\ /258\text{-}R}$ at the same time point. However, we were unable to detect a decrease in the ubiquitin signal surrounding the parasitophorous vacuole membrane (PVM) of intrahepatic *Pb*CSP$^{K\text{-}252\ /258\text{-}R}$ parasites, nor did CUL1 knockdown affect *Pb* CSP ubiquitylation or parasite load in vitro. It is therefore possible that other K moieties within CSP protein, besides K252 and K258, are ubiquitylated by the other families of host E3 ligases.

In this work, we were limited in exploring the type of ubiquitin linkages present in polyubiquitylated CSP. Besides the canonical K48-ubiquitin linked chains associated with proteasomal degradation, the presence of six more lysine residues (K6, K11, K27, K29, K33, and K63) alongside the M1 linkage in ubiquitin molecules creates a staggering variety of homotypic and heterotypic ubiquitin chain elongation[57], each of which has the biochemical capacity to elicit distinct molecular redouts, including protein stability, cellular localization, and interaction with other proteins, DNA, RNA, and autophagy receptors. Given that *Pb* CSP contains over 20 lysine residues, lysine or non-lysine ubiquitin PTM[58], and/or other ubiquitin PTM (such as ubiquitin phosphorylation) may exist and further studies are needed to determine whether such PTMs contribute to this process.

Growing evidence indicates interactions between the parasite interface and host proteins, as PVM is decorated by several autophagy markers, in particular, ubiquitin, LC3, p62, and LAMP1[22–24,59]. We reported that *Pb*CSP$^{K\text{-}252/258\text{-}R}$ parasites present lower infection and higher accumulation of LC3 and LAMP1 during early stages of hepatic infection compared to the control parasite. We also show that the infectivity of the mutant parasite could be reversed by pre-treating cells with chloroquine (CLQ), known to affect the lysosomes-autophagosomes interaction. In our model, we speculate that the loss of ubiquitylated CSP interferes with LC3 machinery and its eventual interaction with lysosomes (LAMP1) at the parasite's PVM leading to parasite elimination by autophagy.

The E3 Cullin-RING Ligases are known to regulate autophagy-related proteins like LC3 and p62[39], albeit we do not observe a clear pattern in the accumulation of p62 at *Pb*CSP$^{K\text{-}252/258\text{-}R}$ parasites membrane suggesting the existence of other mechanisms leading to LAMP1 positive vesicles accumulation at the mutant parasites 4 hpi. However, we could not identify a mechanism to elucidate this connection, which is a limitation of this study. Speculating on how CSP ubiquitylation would aid in escaping autophagic clearance, one possibility is that ubiquitylated CSP acts as a decoy substrate, sequestering host ubiquitylation machinery and preventing the ubiquitylation of key host autophagy-related proteins, eventually interfering with their function. Another possible explanation is the recent observation that CSP increased the proteasomal degradation of LC3B[56]. CSP could potentially bind to LC3B and promote its co- ubiquitylation and co-degradation. Consequently, the block in CSP ubiquitylation would lead to more LC3B available increasing the cell autophagic capacity. However, we favor the first scenario as we did not observe a clear relation between CSP ubiquitylation and degradation.

However, while the CLQ rescue experiment strongly suggests that autophagy contributes to parasite elimination, it does not formally prove this mechanism. CLQ does not directly interfere with autophagosome formation or LC3 recruitment but disrupts lysosomal function downstream of these events and may also influence other cellular pathways. Additional studies, such as genetic inhibition of autophagy-related proteins, will be required to definitively establish the link between *Pb* CSP ubiquitylation and autophagy-mediated parasite clearance.

In the future it would be critical to determine how CSP protein can access the host cytosol and regulate autophagic clearance of the parasite, given it's a parasite plasma membrane protein surrounded by an additional bounding membrane, the PVM. Some studies claim that *Plasmodium* parasites use a PEXEL/VTS motif, localized at the CSP N-terminal region, to translocate CSP into the hepatocyte cytoplasm[60]. However, others were unable to find such a role for PEXEL/VTS motifs, nor its requirement for hepatocyte processing of CSP, thus suggesting that CSP may contain another motif that facilitates its export or it might be exported through a different mechanism used by other intracellular pathogens[61] . Despite the unknown export mechanism, the presence of

CSP within the cytosol of infected hepatocytes has, in fact, been demonstrated in various immunogenic studies focused on pre-erythrocytic *Plasmodium* vaccines. These studies proposed that CD8 + effector T cells recognize CSP-derived antigens on infected hepatocytes, leading to the elimination of the infected cells from the liver[62,63]. These antigens are present in MHC I molecules and need to be processed via the proteasome pathway[64,65].

Furthermore, PVM proteins are shed into the host cytosol, and others have shown this as a mechanism of budding off LC3/LAMP1 from parts of the PVM thereby eluding clearance[23]. The direct incorporation of lipidated host LC3B to the PVM[24] (and binding of other LC3-binding proteins, including ubiquitin and p62[66,67]) is necessary to allow early parasite development. In fact, parasites evade early elimination by autophagy through sequestration of LC3 at the PVM via parasite UIS3, preventing LC3 from binding to other target proteins from the host autophagy machinery[22]. Therefore, another possibility is that the host cell could be ubiquitylating other parasite proteins on the PVM, leading to the known deleterious effects of selective autophagy[22–24,59].

It is worth noting that we cannot rule out the contribution of parasite enzymes in the ubiquitylation of CSP. Unlike salivary gland sporozoites or the blood stage forms which can be obtained in high quantities, liver stage parasites are severely limited in yield, restricting the amount of parasite proteins available for analysis of specific PTMs as ubiquitylation. Indeed, around 80% of *Plasmodium's falciparum* intraerythrocytic proteome exhibits possible targets for ubiquitylation (especially proteins found to be present at the trophozoites and schizont stage)[68]. Given this high prevalence, it is reasonable to assume a similar proportion of "ubiquitylatable" proteins present in early stages of liver infection. However, parasite's protein expression and cellular environment differ significantly between these stages. While the identification of K252 and K258 residues suggests that CSP ubiquitylation is important for parasite survival during the early stages of liver infection, further research is needed to determine the extent and role of CSP ubiquitylation in other parasite life stages, including the mosquito stage, where it remains unclear whether ubiquitylation regulatory mechanisms are active or whether alternative post-translational modifications occur[68]. Further work will also be required to unveil if this mechanism of protection is maintained in the human malaria parasites, such as *P. falciparum*, which also possesses three K residues in the same region of CSP, hinting that these moieties might confer an advantage for other mammalian-infective parasites.

In conclusion, we demonstrate that the loss of *Pb* CSP ubiquitylation at its K252 and K258 moieties leads to increased elimination of *P. berghei* during early stages of liver infection, possibly by autophagy, since we observe an accumulation of the proteins related to autophagy (LC3) and lysosomal responses (LAMP1) in *Pb* CSP lysine-mutant parasites, and interfering with the autophagic pathway lead to intrahepatic parasite's maintenance. These findings expand our understanding of the CSP PTM importance, emphasizing the potential that a deeper knowledge of ubiquitylation during *Plasmodium* exoerythrocytic development may have in the discovery of potential targets for intrahepatic antimalarial intervention[69].

Materials and methods

Mice and ethics statement

BALB/cByJ and C57BL/6 J mice were obtained from Charles River Laboratories International Inc. (Écully, France). Mice were housed at the Instituto de Medicina Molecular (IMM) in a specific pathogen-free environment and given water and food ad libitum, the facility complies with Portuguese law and follows the European Commission recommendations on housing and care of animals and the FELASA (Federation of European Laboratory Animal Science Associations) guidelines concerning laboratory animal welfare. All procedures involving animal experimentation received ethical approval by the Animal Welfare Body of the Instituto de Medicina Molecular (ORBEA-iMM) and were authorized by the Portuguese Competent Authority responsible for the protection of animals used for scientific purposes—Direção Geral de Alimentação e Veterinária (DGAV). All experimental protocols with animals were performed following the guidelines of the national and European regulations. Animals were used at 6–8 weeks of age, both male and female and were randomly assigned to the different experimental groups and in each experiment, animals in experimental groups were matched by age and gender. The number of replicates for all experiments is described in the respective figure legend. No data exclusions are reported and observed variation is reported and contributes to the statistical analysis. ARRIVE guidelines were considered for in vivo experiments data reporting.

Cell lines and mouse primary hepatocytes

Human embryonic kidney (HEK) 293 T (from RRID: CVCL_0063, ATCC®, Manassas, VA, USA) and human hepatoma (HepG2) (from RRID: CVCL_0027, ATCC®, Manassas, VA, USA) cells were cultured in supplemented Dulbecco's modified Eagle's medium (DMEM, Gibco, Thermo Fisher Scientific, Waltham, MA, USA; Cat#21,063–029) and maintained in 5% CO2 humidified incubator at 37°C. DMEM was supplemented with 10% Fetal Bovine Serum (FBS, Gibco, Thermo Fisher Scientific, Waltham, MA, USA, Cat#10500064), 1% L-glutamine and 1% penicillin-streptomycin solutions (Gibco, Thermo Fisher Scientific, Waltham, MA, USA, Cat#15070063), when necessary. Primary murine hepatocytes were isolated from 6–8 weeks old male or female C57BL/6 J mice, as previously described[70]. Liver digestion was obtained with Liberase Blendzyme 3 recombinant collagenase (Roche Diagnostics) and hepatocyte fractionation by 50% Percoll (Sigma Aldrich, Cat#P4937) gradient centrifugation at 70 g for 10 min. Cells were maintained in a 5% CO2 humidified incubator at 37°C in William´s E medium (Gibco, Thermo Fisher Scientific, Waltham, MA, USA Cat#11514466) supplemented with 4% FBS, 2 mM glutamine, 100 U/mL penicillin–streptomycin (Gibco, Thermo Fisher Scientific Waltham, MA, USA), and 0.92 µg/mL Amphotericin B (Gibco), when necessary for later time points.

Plasmids

The plasmid encoding for *Plasmodium berghei* ANKA Circumsporozoite protein (*Pb*CSP) codon-optimized for mammalian expression was commercially synthesized and purified by GeneArt™ (Invitrogen, Thermo Fisher

Scientific). *Pb*CSP sequence was further cloned in pCMV-HA (RRID: Addgene_32530) into the EcoRI and XhoI restriction sites (New England Biolabs, Ipswich, MA, USA), generating pHA-*Pb*CSP^{WT}, and used for the in vitro assays together with a 6xhistidine-tagged ubiquitin plasmid[71] (pHis^{6}-ub), which was kindly provided by Dr. Pedro Simas. Myc-tagged Cullin constructs—pcDNA3-CUL1-Myc, pcDNA3-CUL2-Myc, pcDNA3-CUL3-Myc, pcDNA3-CUL4A-Myc, pcDNA3-CUL4B-Myc and pcDNA3-CUL5-Myc—were commercially obtained from Addgene (plasmid references: 19896, 19892, 19893, 19951, 19922 and 19895, Watertown, MA, USA). For plasmid amplification, XL10 Gold Ultra Competent *E. coli* from Agilent (Santa Clara, CA, USA) and Copy Cutter™ Chemically Competent *E. coli* from Lucigen (Middleton, WI, US) were used and grown in LB Broth. Plasmid DNA was extracted using plasmid DNA extraction kits (NZYtech, Lisbon, Portugal). The plasmids expressing mutant *Pb*CSP with all lysine's (K) substituted by arginine's (R) in the N-terminal, Region I, and C-terminal regions (p*Pb*CSP$^{K\text{-}NT\text{-}R}$, p*Pb*CSP$^{K\text{-}RI\text{-}R}$, p*Pb*CSP$^{K\text{-}CT\text{-}R)}$, and with K to R substitutions in residues 260 and/or 266 (p*Pb*CSP$^{K\text{-}260\text{-}R}$, p*Pb*CSP$^{K\text{-}266\text{-}R}$, and p*Pb*CSP$^{K\text{-}260/266\text{-}R}$) were independently synthesized and cloned into the pCMV-HA backbone by GenScript (Piscataway, NJ, USA). The *PbCSP* gene sequence (Gene ID code *PB*ANKA_0403200) used for the plasmid synthesis was obtained at www.PlasmoDB.org. The recombination vector pCSRep(6) (p*Pb*CSP^{Control}) where *P. berghei* ANKA CSP sequence was substituted by *P. berghei* NK65 CSP, was kindly provided by Photini Sinnis laboratory (Sinnis Laboratory, Johns Hopkins Malaria Research Institute, USA), and used as the basis for the synthesis of the NK65 CSP mutant lysine recombination construct in which K residues 252 and 258 were mutated into R (p*Pb*CSP$^{K\text{-}252\text{-}/258\text{-}R}$). For both plasmids, synthesis and amplification were conducted by GENEWIZ (Leipzig, Germany).

Sporozoite production

The protocol used to achieve salivary glands from infected *Anopheles stephensi* mosquitoes (produced at GIMM Insectarium), has been previously described by our laboratory[49], Sporozoites were freshly dissected into DMEM medium (Gibco), ground with a pestle in 1.5 mL microcentrifuge tubes, and passed through a 40 µm cell-strainer to release sporozoites. Sporozoites were counted using a hemocytometer (Marienfeld Superior, Lauda-Königshofen, Germany). Sporozoites were re-suspended in complete DMEM and added to cells, supplemented, when necessary, with 0,92% Amphotericin B (Gibco, Thermo Fisher Scientific, Waltham, MA, USA, Cat#15290018). Cell plates were then centrifuged at 3000 rpm for 5 min at room temperature followed by incubation at 37°C, 5% CO_2 for the time required according to the experimental set-up.

Parasite lines

Plasmodium parasites used in this study include *P. berghei* ANKA GFP 259 CL2 (referred in the text as *Pb*CSP^{WT}) and *P. berghei* parasite line-507cl[48] (referred in the text GFP-*Pb*WT$^{(ANKA)}$). A double homologous recombination strategy was employed for the generation of the *Pb*NK65 CSP, a novel transgenic parasite line with lysine mutated (*Pb*CSP$^{K\text{-}252/258\text{-}R}$) and the respective control line (*Pb*CSP^{Control}). Transfections were performed on GFP expressing parasite line GFP-*Pb*WT$^{(ANKA)}$ according to a described protocol[48]. Briefly, blood from a BALB/c mouse infected with GFP-*Pb*WT$^{(ANKA)}$ was collected and cultured for 16 h in vitro. Mature schizonts were purified by a Nycodenz (Axis-Shield, Cat#1002424) gradient and transfected with 10 mg of linearized plasmids (p*Pb*CSP^{Control} or p*Pb*CSP$^{K\text{-}252/258\text{-}R}$) using HindIII restriction enzyme (New England Biolabs, Cat#R3104S). Electroporation was obtained by using the Amaxa system (Lonza). Transfected merozoites were injected into the tail vein of a BALB/c mouse and selected with Pyrimethamine provided to animals in drinking water (70 µg/mL). Pyrimethamine-resistant parasite populations containing the correct genomic integration of each construct were cloned by limiting dilution and injection of one parasite per mouse (10 BALB/c male mice, 6–8 weeks of age). Genomic DNA was isolated from the blood of infected animals (Qiagen Total DNA isolation kit) and the successful recombination of the modified *locus* was verified by PCR (NZYTech PCR mix). The oligonucleotides sequences used for genotyping were:

- DP1(from Coppi, et al. 2011): 5'-AATGAGACTATCCCTAAGGG-3';
- DP2 (from Coppi, et al. 2011): 5'- TAATTATATGTTATTTTATTTCCAC-3';
- *Pb*WT locus: 5'- CCTCAATTACAACCAACACATATGCATGTC-3';
- DNA quality fwd: 5'- ATTTGTGTGTATATTCCCC-3';
- DNA quality rev: 5'- TGGTTGTTTCAATTTATTATTAC-3';
- hDHFR fwd: 5'- GGAAGATCTATGGTTGGTTCGCTAAACTGCATCG-3':
- hDHFR rev: 5'- GGAAGATCTTTAATCATTCTTCTCATATACTTC-3'.

Antibodies

Primary antibodies against the following epitopes were used: anti-CSP monoclonal antibody clone 3D11 directed against the repeat region of *P. berghei* CSP (kindly gifted by Miguel Prudêncio from GIMM); mono- and polyubiquitinylated conjugates monoclonal antibody (clone FK2—BML-PW8810-0500; Enzo Life Sciences, Farmingdale, NY, USA); Anti-beta Actin mouse monoclonal antibody (8224; Abcam, Cambridge, UK); Anti-α Tubulin mouse monoclonal antibody (Sigma Aldrich); Anti-Cullin 1 rabbit monoclonal antibody (75812, Abcam); Anti-cMyc Tag mouse monoclonal antibody (MBL lifesciences, Cat# M192-3; RRID: AB_11160947); anti-*Pb*UIS4 goat polyclonal antibody (Sicgen, Cantanhede, Portugal, Cat#AB0042; RRID: AB_2333159), anti-LC3 mouse monoclonal antibody (MBL, M152-3), Anti-LAMP1 rabbit polyclonal antibody (Sigma, L1418); anti-p62 rabbit polyclonal (Sigma-Aldrich, P0067). The secondary antibodies include: Goat anti-mouse IgG F(ab)'2 polyclonal antibody HRP-conjugate (ADI-SAB-100-J; Enzo Life Sciences); Goat anti-rabbit IgG, HRP-linked antibody (A7074; Cell Signaling Technology); Mouse TrueBlot anti-Mouse Ig HRP (eB144; Rockland Immunochemicals), Alexa Fluor 568 dye conjugated donkey Anti-mouse IgG (Thermo Fisher Scientific; Cat# A11057; RRID: AB_2534104), Alexa Fluor 647 dye conjugated donkey Anti-rabbit IgG (Thermo Fisher

Scientific; Cat#A32795, RRID:AB_2762835), Alexa Fluor 488 dye conjugated donkey Anti-goat IgG (Thermo Fisher Scientific, Cat#A32814, RRID:AB_2762838), and Hoechst 33342 (Invitrogen, Carlsbad, CA, USA; Cat# H1399).

Immunoprecipitation assays of infected cells

For total ubiquitin and Cul 1 immunoprecipitation, HepG2 cells were seeded in 24 well-plates (300,000 cells per well), infected with 200,000 to 300,000 *Pb*ANKA^{WT} sporozoites per well. When specified, cells were treated for 8 h with 10 µM of MG132 (starting 4 h prior to infection; Calbiochem, Merck) to inhibit proteasome activity and co-treated for 18 h with 0.3 µM MLN4924 (starting 14 h prior to infection; MedChem Express, NJ 8852, USA) to inhibit neddylation. At 4 hpi, cells were lysed in lysis buffer (50 mM Tris–HCl pH 7.5, 5 mM EDTA, 150 mM NaCl, and 1% Triton X 100), with freshly added protease inhibitors, and left on ice for 1 h. Total cell lysates were incubated overnight at 4 °C on a rotating platform with 10 µg of the respective antibody, anti-LAMP1 antibody previously cross-linked to Protein A/G-plus agarose beads (2003; Santa Cruz Biotechnology, Dallas, TX, USA) and 25% glutaraldehyde (Sigma Aldrich, Cat# G5882)[72]. Total immunoprecipitated proteins were eluted from the beads in 50 µL of 1% sodium dodecyl sulfate (SDS) in phosphate-buffered saline (PBS) and denatured by boiling in Laemmli's buffer (BioRad).ara>

Ni–NTA pull-down ubiquitylation assay

HEK 293 T cells were transiently co-transfected with 3 µg of total plasmid DNA. pCMV-HA empty vector was used to normalize the total DNA amount. Transfections were performed using FuGENE® HD Transfection Reagent according to the manufacturer's instructions (Promega, Maddison, WI, USA). At 40 h post-transfection, cells were treated for 8 h with 10 µM MG132 to block proteasome and preserve ubiquitylated proteins. At 48 h post-transfection (hpi), cells were lysed in 8 M urea buffer with: 10 mM Tris–HCl (pH 7.5), 150 mM NaCl, 1% Triton X-100, 10 mM imidazole, 1 mM Naf , 0,1 mM Na_3VO4 and freshly added protease inhibitors (Roche Complete, EDTA-free; Basel, Switzerland); lysates were incubated with 50 µL of Ni–NTA beads (ThermoFisher Scientific) for 9 h at 4°C, to pull down ubiquitylated proteins. Proteins eluted were denatured by boiling in Laemmli's buffer.

Immunoblotting analysis

For immunoblotting analysis, 8–12% Tris–glycine SDS–polyacrylamide resolving and stacking gels were used under reducing conditions with MiniProtean Tetra Cell equipment (BioRad; Hercules, CA, USA). Running buffer was prepared with 1X Tris/Glycine SDS Buffer (BioRad). Proteins were resolved by electrophoresis at a constant voltage of 80 V until samples entered the resolving gel, voltage was subsequently increased up to 120 V. Resolved proteins were transferred to mixed cellulose transfer membrane (Immobilon-NC HAHY Transfer Membrane, Merk, Darmstadt, Germany) using Biorad system, at 200 mA for 2 h, at 4°C. Membranes were blocked by pre-incubation for 1–2 h at room temperature in PSB with 1% Tween-20 (Sigma Aldrich) and 5% BSA (NZYTech), followed by membrane incubation with respective primary and secondary antibodies. Bound antibodies were visualized using the enhanced chemiluminescence detection system (Immobilon® Western Chemilumonescent HRP Substrate –P90720, MilliporeSigma) and exposed to AGFA® X-ray film (City, Country) in Curix 60 AGFA autoradiography device.

Sporozoites traversal and invasion assessment, in vitro

HepG2 cells were seeded in 24 well plates ($2–3 \times 10^5$ per well) and infected with 150,000 *Pb*CSP^{WT} sporozoites per well. For traversal experiments, Dextran tetramethylrhodamine, 10,000 MW (Thermo Fisher Scientific) was added to the culture[73]. At 2 hpi cells were washed in PBS and detached with trypsin solution (Gibco) for 5 min at 37°C. Cells were re-suspended in 350–500 µl of 10% FBS-PBS solution and analyzed by flow cytometry on the BD Accuri C6 instrument (BD Biosciences, Franklin Lakes, NJ, USA), using appropriate gating based on GFP-expressing signal in FL1 channel (for invasion and infection[74]) and in FL2 channel (for traversal[74]).

Mass spectrometry analysis

HEK 293 T cells were cultured in a 10-cm dish and co-transfected with the following plasmids: 10 µg of pHA-*Pb*CSP^{WT}, 20 µg of pHis^6-ub, and 10 µg of pcDNA3-CUL1-Myc, in the presence of MG132. Forty hours after transfection cells were lysed using a 50 mM Tris–HCl (pH 7.5), 5 mM EDTA, 150 mM NaCl, and 1% Triton X 100 buffer, with freshly added protease inhibitors (Roche Complete, EDTA-free; Basel, Switzerland) and incubated on ice for 45 min. Immunoprecipitation was performed with three different approaches: (i) anti-HA magnetic IP/Co-IP beads kit (88838X; Thermo Scientific), (ii) Protein A/G-plus agarose beads (2003; Santa Cruz Biotechnology) cross-linked to with anti-HA high-affinity rat mAb (clone 3F10; Roche), and (iii) Protein A/G-plus agarose beads cross-linked with 3D11 mAb antibody. The whole eluates (when using anti-HA magnetic IP/Co-IP beads kit) and the beads (when immunoprecipitation was done with antibodies) were sent to the Centre for Genomic Regulation (CRG, Barcelona, Spain) for Mass Spectrometry analysis after trypsin digestion and peptides separation. The proteomics analyses were performed in the CRG/UPF Proteomics Unit, which is part of Proteored, PRB3 and supported by the grant PT17/0019, of the PE I + D + i 2013–2016, funded by ISCIII and ERDF.

Immunofluorescence imaging for sporozoite gliding assessment

Immunofluorescence (IFA) was used to assess gliding of *Pb* sporozoites. In brief, 30,000 sporozoites were allowed to glide in 3D11 mAb (anti-*Pb*CSP antibody) pre-coated glass coverslips in complete DMEM medium for 30 min in a 5% CO2 humidified incubator at 37°C. After this period, coverslips were washed 1 × in PBS, fixed with 4% paraformaldehyde (PFA) (ChemCruyz, Cat# sc-281691) in PBS for 20 min at room temperature,

washed with PBS and stained with 3D11 mAb overnight at 4°C (1:400 in blocking solution; 3% BSA in PBS; BSA obtained from NZYTech). Then, sporozoites were washed 3 times in PBS and incubated for 1.5 h at RT, in a blocking buffer with respective secondary Alexa Fluor antibody. Coverslips were mounted in microscope slides using Fluoromount-G (Invitrogen) and sporozoites-associated trails were observed using Zeiss Cell-Observer Optical Microscope at 40 × magnification.

In vivo liver infection and in vitro parasite burden determination

For ex vivo autophagy inhibition assays, primary hepatocytes were cultured with William´s medium with 100 µM of chloroquine (CLQ)[52] (Sigma Life Sciences, C6628-100G) to block the autophagy flux, for 4 h before infection with sporozoites. To not impair sporozoite traversal and invasion capacity, infections were performed in William´s supplemented with 4% FBS (in the absence of CLQ). At 2 h post-infection, cells were thoroughly washed with PBS and incubated again with William´s without FBS and 100 µM of chloroquine for an additional 2 h, before being processed for subsequent analysis. For the in vivo experiments, mice were infected via intravenous injection of 5×10^3 sporozoites in 200 µL of DMEM and for in vivo autophagy inhibition experiments, mice were treated with 200 µL of 100 µM of chloroquine[24] (Sigma Life Sciences, C6628-100G) in 0.9% NaCl at 24 and 2 h prior to sporozoite infection. At 4 and 44 h after sporozoite infection, livers of infected mice were collected into 3 mL of denaturing solution: 4 M guanidium thiocyanite (Sigma), 25 mM sodium citrate (Sigma), 0.5% sarcosyl (Sigma) in MilliQ water treated with DEPC (Sigma). Livers were then mechanically homogenized using 1 mm diameter silica beads (BioSpec Products, Bartlesville, OK, USA) in MiniBeadBeater homogenizer (BioSpec Products) for 2 min. After mechanical disruption of the tissue, total RNA was extracted from 200 µL of tissue lysate using the NZY Total RNA Isolation Kit (NZYTtech) following the manufacturer's instructions. Quantification of total RNA concentration was performed on NanoDrop 2000 spectrophotometer (Thermo Fisher Scientific) according to the manufacturer´s guidelines. 500–1000 ng of total mRNA was used for tandem cDNA synthesis and amplification in an RT-PCR 7500 Fast cycler (Applied Biosystems) with One-step NZYSpeedy RT-qPCR Probe kit (NZYtech) and primer/probe set specific for *P. berghei* 18 s gene. For cells in culture (either HepG2 or mouse primary hepatocytes), cells were lysed, with lysis buffer from NZY Total RNA Isolation Kit (NZYtech), supplemented with 1% v/v β-mercaptoethanol. RNA was extracted and quantified as above. 500–1000 ng of total RNA from each sample was reversely transcribed into cDNA using a cDNA kit (NZYTech). Quantitative amplification was performed on ViiA 7 or 7500Fast Real-Time PCR Systems (Applied Biosystems). The relative expression of *P. berghei* 18 s gene was quantified using the comparative ΔΔCT method[49]. M. musculus hypoxanthine–guanine phosphoribosyl transferase (Hprt) served as the normalizing reference gene. The oligonucleotides sequences used for qPCR are:

- *Pb*18s_fwd: 5'- AAGCATTAAATAAAGCGAATACATCCTTAC-3';
- *Pb*18s_rev: 5'- GGAGATTGGTTTTGACGTTTATGTG;
- MmHprt_fwd: 5'- TTTGCTGACCTGCTGGATTAC-3';
- MmHprt_rev: 5'- CAAGACATTCTTTCCAGTTAAAGTTG-3' (for SYBR Green assay);
- *Pb*18s_fwd: 5'- AGGGAGCCTGAGAAATAG-3';
- *Pb*18s_rev: 5'- GTCACTACCTCTCTTATTTAGAA-3';
- *Pb*18s Probe: 5'- FAM-ACCACATCTAAGGAAGGCAGCA-BHQ1-3';
- MmHprt_fwd: 5'- GAACCAGGTTATGACCTA-3';
- MmHprt_rev: 5'- TCTCCTTCATGACATCTC-3';
- MmHprt Probe: 5'- FAM-TTCAGTCCTGTCCATAATCAGTCCAT-BHQ1-3';
- MmCullin1_fwd: 5'- GAGGCAGAACTAGAAGAC-3';
- MmCullin1_rev: 5'-CTTGCTTTAACTTGGAGATC-3';
- MmCullin1 Probe: 5'- FAM-TCAGCATCGTCACTCGCACT-BHQ1-3' (for TaqMan probe assay).

Gene silencing with RNA interference

Murine primary hepatocytes were reverse-transfected with ON-TARGET plus Human CUL1 siRNA—SMARTpool siRNA (Dharmacon, Horizon Discovery Ltd), as previously described[22], using the Lipofectamine RNAiMax transfection reagent (Life Technologies) according to the manufacturer's instructions. Non-targeting SMARTpool siRNA was used as a negative control (Dharmacon, Horizon Discovery Ltd). Infections were performed 24 h after transfection, and knockdown efficiency was assessed by qRT–PCR at 4 h post-infection. Gene expression levels were normalized against those of hypoxanthine–guanine phosphoribosyl transferase (Hprt1; listed above).

Immunofluorescence imaging of infected primary hepatocytes

Immunofluorescence analysis to calculate the % of invaded sporozoites by accessing the intracellular localization of CSP on primary hepatocytes was performed using a previously published[75] in-and-out staining protocol. Primary murine hepatocytes were seeded on glass coverslips on 24-well plates and infected with *Pb*CSP^{Control} or *Pb*CSP$^{K\text{-}252/258\text{-}R}$ sporozoites. At 2 hpi, medium was removed, cells were fixed with 4% paraformaldehyde and then blocked with 1% BSA in PBS. The extracellular/transmigrating parasites were revealed by incubation with mAb 3D11 followed by donkey anti-mouse Ig conjugated to Alexa 568. To reveal the sporozoites inside intact cells (intracellular sporozoites) in the same experiment, the cells were then permeabilized with methanol, and all parasites (intra- and extracellular) were revealed by incubating the samples again with 3D11 mAb followed by donkey anti-mouse Ig conjugated to Alexa 488. Coverslips were mounted on microscope slides with Fluoromount G (SouthernBiotech, Birmingham, AL, USA). Images were acquired in an inverted Zeiss Cell-Observer Optical Microscope (ZEISS, Germany) and in a Zeiss LSM 980 confocal microscope (Carl Zeiss,

Oberkochen, Germany), both with 40 × magnification. The percentage of invasion was calculated from the following equation:

$$\frac{numberofintracellularspz}{numberofintracellularspz + numberofextracellularspz} = \%ofinvadedsporozoites$$

Statistical analysis

BD Accuri data analysis was performed using FlowJo X software (FlowJo LLC, Ashland, OR USA). All immunofluorescence images were processed using FIJI software (version 1.52i)[76] and macros written for each analysis to automate it[72]. For Western Blot images quantification, the software Adobe Photoshop was used. All data presented was plotted and statistically analyzed in GraphPad Prism 5 software (GraphPad, La Jolla, CA). Mann–Whitney *U* test was used to assess the significance of the differences observed between the two groups.

Data availability

The present study has generated novel plasmids which are available for sharing upon personal communication. Requests should be submitted to the Lead Contact, Maria M. Mota (maria.mota@gimm.pt). All data needed to evaluate the conclusions in the paper are present in the main text and/or the appendix materials. This study includes no data deposited in external repositories.

Received: 26 November 2024; Accepted: 10 April 2025
Published online: 25 April 2025

References

1. WHO. *World Malaria Report 2018*. (2018). ISBN 978 92 4 1564403.
2. Prudêncio, M., Rodriguez, A. & Mota, M. M. The silent path to thousands of merozoites: the Plasmodium liver stage. *Nat Rev Microbiol* **4**, 849–856 (2006).
3. Escalante, A. A. & Ayala, F. J. Phylogeny of the malarial genus Plasmodium, derived from rRNA gene sequences. *Proc Natl Acad Sci U S A* **91**, 11373–11377 (1994).
4. Mccutchan, T. F. *et al.* Comparison of circumsporozoite proteins from avian and mammalian malarias : Biological and phylogenetic implications. *Proc. Natl. Acad. Sci.* 11889–11894 (1996).
5. Ménard, R. et al. Circumsporozoite protein is required for development of malaria sporozoites in mosquitoes. *Nature* **385**, 336–340 (1997).
6. Coppi, A. et al. The malaria circumsporozoite protein has two functional domains, each with distinct roles as sporozoites journey from mosquito to mammalian host. *J Exp Med* **208**, 341–356 (2011).
7. Frevert, U. et al. Malaria Circumsporozoite Protein Binds to Heparan Sulfate Proteoglycans Associated with the Surface Membrane of Hepatocytes. *J. Exp. Med.* **177**, 1287–1298 (1993).
8. Kojin, B. B. et al. Endogenously-expressed NH 2 -terminus of circumsporozoite protein interferes with sporozoite invasion of mosquito salivary glands. *Malar J* **15**, 1–11 (2016).
9. Rathore, D. et al. An immunologically cryptic epitope of Plasmodium falciparum circumsporozoite protein facilitates liver cell recognition and induces protective antibodies that block liver cell invasion. *J. Biol. Chem.* **280**, 20524–20529 (2005).
10. Coppi, A., Pinzon-Ortiz, C., Hutter, C. & Sinnis, P. The Plasmodium circumsporozoite protein is proteolytically processed during cell invasion. *J Exp Med* **201**, 27–33 (2005).
11. Nussenzweig, V. & Nussenzweig, R. S. Rationale for the Development of an Engineered Sporozoite Malaria Vaccine. *Adv Immunol* **45**, 283–334 (1989).
12. Ferguson, D. J. P. et al. The repeat region of the circumsporozoite protein is critical for sporozoite formation and maturation in Plasmodium. *PLoS ONE* **9**, 1–25 (2014).
13. Wang, Q., Fujioka, H. & Nussenzweig, V. Mutational analysis of the GPI-anchor addition sequence from the circumsporozoite protein of Plasmodium. *Cellular Microbiolog* **7**, 1616–1626 (2005).
14. Vozandychova, V., Stojkova, P., Hercik, K., Rehulka, P. & Stulik, J. The ubiquitination system within bacterial host-pathogen interactions. *Microorganisms* **9**, 1–22 (2021).
15. Kumar, R., Mehta, D., Mishra, N., Nayak, D. & Sunil, S. Role of host-mediated post-translational modifications (PTMS) in RNA virus pathogenesis. *Int J Mol Sci* **22**, 1–26 (2021).
16. Weil, R. Does antigen masking by ubiquitin chains protect from the development of autoimmune diseases?. *Front Immunol* **5**, 1–13 (2014).
17. Johnson, N. & Philip, N. Beyond phosphorylation: Putative roles of post-translational modifications in Plasmodium sexual stages. *Mol Biochem Parasitol* **245**, 111406 (2021).
18. Wang, J. et al. Protein modification characteristics of the malaria parasite plasmodium falciparum and the infected erythrocytes. *Mol. Cell. Proteomics* **20**, 100001 (2021).
19. Rashidi, S. et al. The main post-translational modifications and related regulatory pathways in the malaria parasite Plasmodium falciparum: An update. *J Proteomics* **245**, 10429 (2021).
20. Green, J. L. et al. Ubiquitin activation is essential for schizont maturation in Plasmodium falciparum blood-stage development. *PLoS Pathog* **16**, 1–29 (2020).
21. Swearingen, K. E. et al. Interrogating the Plasmodium Sporozoite Surface: Identification of Surface-Exposed Proteins and Demonstration of Glycosylation on CSP and TRAP by Mass Spectrometry-Based Proteomics. *PLoS Pathog* **12**, 1–32 (2016).
22. Real, E. et al. Plasmodium UIS3 sequesters host LC3 to avoid elimination by autophagy in hepatocytes. *Nat Microbiol* **3**, 17–25 (2017).
23. Agop-Nersesian, C. et al. Shedding of host autophagic proteins from the parasitophorous vacuolar membrane of Plasmodium berghei. *Sci Rep* **7**, 1–14 (2017).
24. Prado, M. et al. Long-term live imaging reveals cytosolic immune responses of host hepatocytes against plasmodium infection and parasite escape mechanisms. *Autophagy* **11**, 1561–1579 (2015).
25. Mello-Vieira, J., Bopp, T. & Dikic, I. Ubiquitination and cell-autonomous immunity. *Curr Opin Immunol* **84**, 102368 (2023).
26. Kocaturk, N. M. & Gozuacik, D. Crosstalk between mammalian autophagy and the ubiquitin-proteasome system. *Front Cell Dev Biol* **6**, 1–27 (2018).
27. Yin, Z., Popelka, H., Lei, Y., Yang, Y. & Klionsky, D. J. The Roles of Ubiquitin in Mediating Autophagy. *Cells* **9**, 1–31 (2020).
28. Pohl, C. & Dikic, I. Cellular quality control by the ubiquitin-proteasome system and autophagy. *Science* **1979**(366), 818–822 (2019).

29. Cheng, X. T. et al. Revisiting LAMP1 as a marker for degradative autophagy-lysosomal organelles in the nervous system. *Autophagy* **14**, 1472–1474. https://doi.org/10.1080/15548627.2018.1482147 (2018).
30. Kisselev, A. F. & Goldberg, A. L. Proteasome inhibitors: From research tools to drug candidates. *Chem Biol* **8**, 739–758 (2001).
31. Pang, Y. et al. Evolution from covalent conjugation to non-covalent interaction in the ubiquitin-like ATG12 system. *Nat Struct Mol Biol* **26**, 289–296 (2019).
32. Rodrigues, L., Popov, N., Kaye, K. M. & Simas, J. P. Stabilization of Myc through Heterotypic Poly-Ubiquitination by mLANA Is Critical for γ-Herpesvirus Lymphoproliferation. *PLoS Pathog* **9**, (2013).
33. Kliza, K. & Husnjak, K. Resolving the Complexity of Ubiquitin Networks. *Front Mol Biosci* **7**, (2020).
34. Liu, Y. C., Penninger, J. & Karin, M. Immunity by ubiquitylation: A reversible process of modification. *Nat Rev Immunol* **5**, 941–952 (2005).
35. Bedford, L., Lowe, J., Dick, L. R., Mayer, R. J. & Brownell, J. E. Ubiquitin-like protein conjugation and the ubiquiting-proteasome system as drug targets. *Nat Rev Drug Discov* **10**, 29–46 (2011).
36. Berndsen, C. E. & Wolberger, C. New insights into ubiquitin E3 ligase mechanism. *Nat Struct Mol Biol* **21**, 301–307 (2014).
37. Zhou, Q. & Sun, Y. MLN4924: additional activities beyond neddylation inhibition. *Mol Cell Oncol* **6**, 1–3 (2019).
38. Nguyen, H. C., Wang, W. & Xiong, Y. Cullin-RING E3 ubiquitin ligases: Bridges to destruction. *Subcell Biochem* **83**, 323–347 (2017).
39. Cui, D., Xiong, X. & Zhao, Y. Cullin-RING ligases in regulation of autophagy. *Cell Div* **11**, 1–14 (2016).
40. Zhou, W., Wei, W. & Sun, Y. Genetically engineered mouse models for functional studies of SKP1-CUL1-F-box-protein (SCF) E3 ubiquitin ligases. *Cell Res.* **23**, 599–619. https://doi.org/10.1038/cr.2013.44 (2013).
41. Doud, M. B. et al. Unexpected fold in the circumsporozoite protein target of malaria vaccines. *Proc. Natl. Acad. Sci.* **109**, 7817–7822 (2012).
42. Nussenzweig, V. & Nussenzweig, R. S. Circumsporozoite proteins of malaria parasites. *Cell* **42**, 401–403 (1985).
43. Dundas, K., Shears, M. J., Sinnis, P. & Wright, G. J. Important Extracellular Interactions between Plasmodium Sporozoites and Host Cells Required for Infection. *Trends. Parasitol.* **35**, 129–139 (2019).
44. Rashpa, R., Klages, N., Schvartz, D., Pasquarello, C. & Brochet, M. The Skp1-Cullin1-FBXO1 complex is a pleiotropic regulator required for the formation of gametes and motile forms in Plasmodium berghei. *Nat. Commun.* https://doi.org/10.1038/s41467-023-36999-8 (2023).
45. Udeshi, N. D., Mertins, P., Svinkina, T. & Carr, S. A. Large-scale identification of ubiquitination sites by mass spectrometry. *Nat Protoc* **8**, 1950–1960 (2013).
46. Udeshi, N. D., Mertins, P., Svinkina, T. & Carr, S. A. Large-scale identification of ubiquitination sites by mass spectrometry. *Nat. Protoc.* **8**, 1950–1960 (2013).
47. Coppi, A. et al. The malaria circumsporozoite protein has two functional domains, each with distinct roles as sporozoites journey from mosquito to mammalian host. *J. Exp. Med.* **208**, 341–356 (2011).
48. Janse, C. J., Ramesar, J. & Waters, A. P. High-efficiency transfection and drug selection of genetically transformed blood stages of the rodent malaria parasite Plasmodium berghei. *Nat. Protoc.* **1**, 346–356 (2006).
49. Mello-Vieira, J., Enguita, F. J., de Koning-Ward, T. F., Zuzarte-Luís, V. & Mota, M. M. Plasmodium translocon component EXP2 facilitates hepatocyte invasion. *Nat. Commun.* https://doi.org/10.1038/s41467-020-19492-4 (2020).
50. Grumati, P. & Dikic, I. Ubiquitin signaling and autophagy. *J. Biol. Chem* **293**, 5404–5413 (2018).
51. Gómez-díaz, C. & Ikeda, F. Roles of ubiquitin in autophagy and cell death. *Semin. Cell. Dev. Biol.* https://doi.org/10.1016/j.semcdb.2018.09.004 (2018).
52. Mauthe, M. et al. Chloroquine inhibits autophagic flux by decreasing autophagosome-lysosome fusion. *Autophagy* **14**, 1435–1455 (2018).
53. Swearingen, K. E. *et al. Proteogenomic Analysis of the Total and Surface-Exposed Proteomes of Plasmodium Vivax Salivary Gland Sporozoites*. *PLoS Neglected Tropical Diseases* vol. 11 (2017).
54. Lopaticki, S. *et al.* Protein O-fucosylation in Plasmodium falciparum ensures efficient infection of mosquito and vertebrate hosts. *Nat Commun* **8**, (2017).
55. Zheng, H. et al. ATG Ubiquitination Is Required for Circumsporozoite Protein to Subvert Host Innate Immunity Against Rodent Malaria Liver Stage. *Front. Immunol.* **13**, 1–15 (2022).
56. Lu, X. et al. Plasmodium Circumsporozoite Protein Enhances the Efficacy of Gefitinib in Lung Adenocarcinoma Cells by Inhibiting Autophagy via Proteasomal Degradation of LC3B. *Front. Cell Dev. Biol.* **10**, 1–16 (2022).
57. French, M. E., Koehler, C. F. & Hunter, T. Emerging functions of branched ubiquitin chains. *Cell Discov.* **7**(1), 6 (2021).
58. Engström, P., Burke, T. P., Tran, C. J., Iavarone, A. T. & Welch, M. D. Lysine methylation shields an intracellular pathogen from ubiquitylation and autophagy. *Sci. Adv.* **7**(26), 2517 (2021).
59. Niklaus, L. et al. Deciphering host lysosome-mediated elimination of Plasmodium berghei liver stage parasites. *Sci. Rep.* **9**, 1–15 (2019).
60. Singh, A. P. et al. Plasmodium Circumsporozoite Protein Promotes the Development of the Liver Stages of the Parasite. *Cell* **131**, 492–504 (2007).
61. Cockburn, I. A. et al. Dendritic cells and hepatocytes use distinct pathways to process protective antigen from Plasmodium in vivo. *PLoS Pathog.* **7**(3), e1001318 (2011).
62. Chakravarty, S. et al. CD8+ T lymphocytes protective against malaria liver stages are primed in skin-draining lymph nodes. *Nat. Med.* **13**, 1035–1041 (2007).
63. Balam, S., Romero, J. F., Bongfen, S. E., Guillaume, P. & Corradin, G. CSP-A model for in vivo presentation of plasmodium berghei sporozoite antigens by hepatocytes. *PLoS ONE* **7**(12), e51875 (2012).
64. Bongfen, S. E., Torgler, R., Romero, J. F., Renia, L. & Corradin, G. Plasmodium berghei -infected primary hepatocytes process and present the circumsporozoite protein to specific CD8+ T Cells In Vitro. *J. Immunol.* **178**, 7054–7063 (2007).
65. Bongfen, S. E., Balam, S., Torgler, R., Romero, J. F. & Corradin, G. Processing of the circumsporozoite protein in infected hepatocytes is not dependent on aspartic proteases. *Parasite Immunol.* **30**, 375–378 (2008).
66. Schmuckli-Maurer, J. et al. Inverted recruitment of autophagy proteins to the Plasmodium berghei parasitophorous vacuole membrane. *PLoS ONE* **12**(8), e0183797 (2017).
67. Wacker, R. *et al.* LC3-association with the parasitophorous vacuole membrane of Plasmodium berghei liver stages follows a noncanonical autophagy pathway. *Cell. Microbiol* .**19**, (2017).
68. Ponts, N. et al. Unraveling the ubiquitome of the human malaria parasite. *J. Biol. Chem.* **286**, 40320–40330 (2011).
69. Lindenthal, C., Weich, N., Chia, Y. S., Heussler, V. & Klinkert, M. Q. The proteasome inhibitor MLN-273 blocks exoerythrocytic and erythrocytic development of Plasmodium parasites. *Parasitology* **131**, 37–44 (2005).
70. Amichay Afriat, Vanessa Zuzarte-Luís, Keren Bahar Halpern, Lisa Buchauer, Sofia Marques, Aparajita Lahree, Ido Amit, Maria M. Mota, S. I. *A Spatiotemporally Resolved Single Cell Atlas of the Plasmodium Liver Stage*. https://doi.org/10.1101/2021.12.03.471111.
71. Treier, M., Staszewski, L. M. & Bohmann, D. Ubiquitin-dependent c-Jun degradation in vivo is mediated by the δ domain. *Cell* **78**, 787–798 (1994).
72. Lahree, A. et al. Active APPL1 sequestration by Plasmodium favors liver-stage development l. *Cell. Rep.* **39**, 1–16 (2022).
73. Prudêncio, M., Rodrigues, C. D., Ataíde, R. & Mota, M. M. Dissecting in vitro host cell infection by Plasmodium sporozoites using flow cytometry. *Cell Microbiol.* **10**, 218–224 (2008).
74. Prudêncio, M., Mota, M. M. & Mendes, A. M. A toolbox to study liver stage malaria. *Trends. Parasitol.* **27**, 565–574 (2011).

75. Rénia, L. et al. Malaria sporozoite penetration A new approach by double staining. *J. Immunol. Methods* **112**, 201–205 (1988).
76. Schindelin, J. et al. Fiji: An open-source platform for biological-image analysis. *Nat. Methods.* **9**, 676–682 (2012).

Acknowledgements
We thank Miguel Prudêncio (GIMM, Lisbon, Portugal) for kindly providing the 3D11 mAb (anti-P. berghei CSP antibody) and to Photini Sinnis (Johns Hopkins Malaria Institute, Baltimore, USA) for kindly providing the pCSRep recombination vector. We also thank Ana Parreira for producing *P. berghei*-infected *Anopheles* mosquitos, Viriato M´Bana for assistance with mosquito salivary gland dissection, Vanessa Morais (GIMM, Lisbon, Portugal) for providing guidelines on cross-linked immunoprecipitation assays, and the Flow Cytometry, BioImaging and Rodent Facilities teams (GIMM, Portugal) for assistance. A special thank you to Photini Sinnis and Nisha Philip for critically revising the manuscript. This work was supported by grants from the la Caixa Foundation (HR17-00264 and HR23-00499) and Fundação para a Ciência e Tecnologia (FCT) (PTDC/SAU-MIC/113697/2009 and PTDC/SAU-PAR/30751/2017 to V.Z.L. and M.M.M respectively). S.J.S.B was sponsored by FCT fellowship SFRH/BD/114464/2016 and IMM research fellowship IMM/BII/8-2020. A.L. and J.M.V were sponsored by FCT (PD/BD/114036/2015 and SFRH/BD/52226/2013 respectively).

Author contributions
Conceptualization: Initial concept V.Z.L., development and further conceptualization S.J.S.B. with the assistance of A.M.; Investigation: S.J.S.B., A.L., S.M., I.B. and A.M. performed the experiments and S.J.S.B., A.M. and A.L. analyzed and processed the data.; Writing – Original draft: S.J.S.B., A.L., A.M. and J.M.V. Writing – Review and Editing: S.J.S.B., S.M., A.M., J.M.V., A.L. and M.M.M.

Declarations

Competing interests.
The authors declare no competing interests.

Additional information
Supplementary Information The online version contains supplementary material available at https://doi.org/10.1038/s41598-025-98294-4.

Correspondence and requests for materials should be addressed to M.M.M.

Reprints and permissions information is available at www.nature.com/reprints.

Publisher's note Springer Nature remains neutral with regard to jurisdictional claims in published maps and institutional affiliations.